Sigma J Eng Nat Sci, Vol. 44, No. 2, pp. 820–842, April, 2026

Sigma Journal of Engineering and Natural Sciences
Web page info: https://sigma.yildiz.edu.tr
DOI: 10.14744/sigma.2026.2014

Research Article

Exploring fractional dynamics of fourth order parabolic partial differential equations with power law Kernel

Shelly ARORA[1], Wenxiu MA[2,3,4,5,*], Sukhjit SINGH DHALIWAL[6], Atul PASRIJA[1]

[1]*Department of Mathematics, Punjabi University, Patiala 147002, India*
[2]*Department of Mathematics, Zhejiang Normal University, Jinhua 321004, Zhejiang, China*
[3]*Research Center of Astrophysics and Cosmology, Khazar University, Baku 1096, Azerbaijan*
[4]*Department of Mathematics and Statistics, University of South Florida, Tampa, 33620-5700, USA*
[5]*Material Science Innovation and Modelling, Department of Mathematical Sciences, North-West University, Mmabatho, 2735, South Africa*
[6]*Department of Mathematics, SLIET, Longowal, Sangrur, Punjab, 148106, India*

ARTICLE INFO

Article history
Received: 20 November 2024
Revised: 02 January 2025
Accepted: 28 January 2025

Keywords:
Fourth-Order Parabolic Equations; GB Transform; Homotopy Perturbation Method; Liouville-Caputo Fractional Derivative

ABSTRACT

The aim of this study is to establish an efficient method for exploring the fractional dynamics of fourth-order parabolic partial differential equations. The generalized bivariate homotopy perturbation method is suggested to determine expansion solutions for the considered models. This scheme decomposes non-linearity using He's polynomials. It is applied within the non-local fractional framework of Liouville-Caputo sense. The impact of fractional phenomena is briefly described. A comparative analysis of the suggested scheme is presented through graphical and tabular illustrations. Error analysis, based on the evaluation of absolute error, demonstrates the high precision, authenticity, and superiority of the suggested scheme. The existence and uniqueness of continuous solutions are shown for the fractional variants of Cauchy problems. The semi-analytic results obtained from the suggested scheme effectively capture the wave dynamics of physical systems across various physical parameters. The proposed algorithm does not rely on the availability of an exact solution to demonstrate its efficacy.

Cite this article as: Arora S, Ma W, Singh Dhaliwal S, Pasrija A. Exploring fractional dynamics of fourth order parabolic partial differential equations with power law Kernel. Sigma J Eng Nat Sci 2026;44(2):820–842.

INTRODUCTION

The dynamical behavior of fourth-order parabolic equations has attracted global interest. These equations can be framed by non-linear functional equations defined by:

$$w = g + \mathrm{M}(w, w_{\eta}, w_{\xi}, w_{\xi\xi}, w_{\xi,\xi,\xi}, w_{\xi\xi\xi\xi})$$

where g is the known function and M is the non-linear operator.

*Corresponding author.
*E-mail address: mawx@cas.usf.edu, atulpasrija_rs@pbi.ac.in

This paper was recommended for publication in revised form by Editor-in-Chief Ahmet Selim Dalkilic

The first-order derivative w_ξ reflects the advective transport. The term $w_{\xi\xi}$ accounts for instability at large scales. The inclusion of the third-order term $w_{\xi\xi\xi}$ yields dispersion effect. The fourth-order term $w_{\xi\xi\xi\xi}$ provides exponential damping out of very sharp spikes at small scales, and the non-linear term stabilizes the system dynamics by transferring energy between large and small scales.

In the past few decades, theoretical study and practical simulation have been addressed via fractional operators [1-4]. These operators have been found to be better predictors than integer-order models. Fractional operators have emerged as a non-local tool for providing an excellent description of a real evolution process with memory and hereditary properties. It naturally arises in multiple conducts of wave phenomena, exhibiting chaos in wave motions, solitons, wrinkled flame front propagation, phase turbulence in reaction-diffusion systems, and chaotic drifting waves induced by photon collision [5-10]. However, the inclusion of fractional derivatives with variable and non-variable order demands highly influential analytic tools. For numerical treatment, it requires a large number of variables to cope with reality. The implementation of fractional operators can be found in a wide range of fields such as electromagnetism, bioengineering, signal processing, optimal control theory, and finance [7-14].

There are innumerable alternative definitions of fractional operators available in the literature [11-15]. Although the Liouville-Caputo (L-C) derivative and the Riemann-Liouville (R-L) derivative are the most frequently used terminologies. With the definition of Caputo fractional derivative, a fractional derivative would be applicable for differentiable functions only. To deal with non-differentiable functions, R-L derivative is preferred, but it denies being zero for constant functions. To address non-local and non-singular kernel properties, the Caputo-Fabrizio (C-F) and Atangana Baleanu in Caputo sense (ABC) serve as extensions of the L-C operator. However, there are certain drawbacks when employing a non-singular fractional differential operator. The inability of a fractional differential operator with a non-singular kernel to satisfy the fundamental theorem of fractional calculus has been documented by Diethelm [16]. Another notion of local fractional derivatives extends the familiar limit definition of the classical derivative [17,18]. Because of their simplicity, the local fractional derivatives can meet a large number of well-known aspects of classical derivatives, such as the chain rule, quotient rule, integration by parts, Gronwall's inequality, fractional series representation of functions, and so on. However, the inclusion of the memory effect falls outside the scope of local fractional derivatives.

In present study, renowned models of fourth order partial differential equations featured with Caputo derivative are considered as:

- Fractional generalized Kuramoto-Sivashinsky (FGKS) equation:

$$C_\eta^\alpha w + ww_\xi + xw_{\xi\xi} + yw_{\xi\xi\xi} + zw_{\xi\xi\xi\xi} = 0. \quad (1)$$

- Fractional Swift-Hohenberg (FSH) equation without dispersion:

$$C_\eta^\alpha w + w_{\xi\xi\xi\xi} + 2w_{\xi\xi} + (1-x)w + w^3 = 0, 0 < x \leq 1. \quad (2)$$

- Fractional Swift-Hohenberg equation (FSH) with dispersion:

$$C_\eta^\alpha w + w_{\xi\xi\xi\xi} + 2w_{\xi\xi} - xw_{\xi\xi\xi} - yw - 2w^2 + w^3 = 0. \quad (3)$$

- Fractional Cahn-Hilliard (FCH) equation:

$$C_\eta^\alpha w = xw_\xi + \left(-w_{\xi\xi} - w + w^3\right)_{\xi\xi}, \quad (4)$$

or

$$C_\eta^\alpha w = xw_\xi + 6w\left(w_\xi\right)^2 + 3w^2w_{\xi\xi} - w_{\xi\xi} - w_{\xi\xi\xi\xi}, \quad (5)$$

where x and y are real constantss.

For α = 1, Equation 1 represents the classical generalized Kuramoto-Sivashinsky (GKS) equation [19]. The variants of GKS equation have been extensively explored with different initial and boundary data by numerous analytic and numerical tools, such as homotopy perturbation method [20] and homotopy analysis method, which have been projected to treat space fractional GKS equation [21], residual power series method has been implemented with the projection of Riemann-Liouville integral and Caputo's fractional framework [22], the amalgamation of the integral transform with variational iteration method [23] and q-HAM [24] are used to construct semi-analytic expansion solutions. The *G'/G* expansion method [25,26], exp-function method [27], modified Kudryashov method [28], tanh method and its extended version [29,30] are employed to interpret various soliton conductance. The non-integrability of K-S equation has been established via Painleve analysis [31]. The rich characterization of several dynamics of K-S model, such as multimodal, cellular, oscillatory, and chaotic solutions, have been studied so far [32-35].

In 1977, Jack Swift and Pierre Hohenberg have introduced and nurtured Swift-Hohenberg (S-H) equation as a universal model for the temperature and fluid velocity dynamics of convection [36]. S-H equation intrinsically occurs in nano-crystalline materials for expressing the average density of detachment during creation of shear microbands [37]. S-H equation addresses numerous issues such as patterns in Rayleigh-Bernard convections, patterns within thin vibrated granular layers, defect dynamics, spatial-temporal chaos and study of lasers [38-43]. S-H equation demonstrates the mechanism of amplitude of optical electrical field within the cavity embodying a non-linear medium [44]. Application of S-H equation rangs in the theory of pattern formation in fluid layers confined between horizontal well-conducting boundaries [45] Several researchers have conducted analytic and numerical experiments to unveil the dynamics of S-H equation. [46]

provides evidence for the existence of quasi-patterns for the S-H equation. With inclusion of dispersive effect, in [47] authors have reported the achievement of spatial reversibility. In [48], investigators have proved the existence of non-stationary meromorphic solutions of S-H equation. Consequently, they have derived the simple periodic and elliptic non-stationary travelling wave solutions of S-H equation. Semi-analytic techniques [49-52] are eminently aided to interpret the behavior of S-H equation.

The Cahn-Hilliard (C-H) equation is a non-linear, stiff, fourth-order parabolic equation. It shows how the conserved field has changed over time. In essence, the C-H equation has been created to simulate the spinodal breakdown of a binary system at a specific temperature. It records both a very gradual coarsening, which results in bulk phases with an interface separating them, and a quick phase separation, which creates a thin interface between two phases. The C-H equation has been solved by many researchers using various time discretization and spatial techniques. The C-H equation has been examined in 2D form by Grasselli et al. [53], who have established a number of findings about the well-posedness and large-time behavior of solutions. Analysis has been done in the presence of bounded absorbing sets in two distinct phase spaces. Additionally, the existence of exponential and global attractors has been proven. The proposed C-H equation has been solved by Lee et al. [54] utilizing the pseudo-spectral, finite element, and finite difference methods. Together with first- and second-order temporal algorithms, Chen et al. [55] have suggested a finite difference technique for the C-H system with a logarithmic Flory Huggins energy potential. For the C-H and Allen-Cahn equations, Zhang et al. [56] have suggested the optimal control issue. For optimum control issues, the optimality requirements have been applied. The C-H Biot model has been suggested by Storvik et al. [57] to describe flow through deformable porous media. Biot's theory has controlled the coupling between flow and deformation, resulting in a three-way coupled system. In [58], Manzenaro et al. have addressed a C-H model with wall boundary conditions. Using a curvilinear hexahedral model, the model equations have been discretized by the discontinuous Galerkin spectral element approach. The first-order implicit-explicit technique, which separated the system into two C-H equations, has been used to explore the discretization of time. For the space-time fractional order C-H equation, Khan et al. [59] have presented the traveling wave solution using the auxiliary approach. For complex dynamics, Zhou and Xie [60] have presented a multicomponent three-dimensional C-H equation. Using the projected gradient approach, lagrangian multiples of Gibbs *n* simplex phase constraints have been computed.

In its versatile framework, the present study incorporates potential models (FGKS, FSH and FCH) of thermal science, material science, biological science, hydrodynamics, study of lasers, oceanography and many more. The blend of these subjects forms the basis of vast studies in engineering and natural sciences. Therefore, the choice of FGKS, FSH and FCH equations will engage the interest of a large part of the scientific community. Despite the numerous semi-analytic studies for L-C fractional GKS, S-H and C-H equations, the establishment of reliability of solutions for $0 < \alpha < 1$ is extensively unexplored. While addressing this gap through proposing the first-time application of the generalized bivariate homotopy perturbation method (GB-HPM) for fourth-order equations, the present study demonstrates the competence of GB-HPM in terms of accuracy.

The manuscript is organized in the given manner. Section 1 is based on the introduction of the theory and applications of the considered problems. In Section 2, definitions, properties and terminologies of L-C derivative and generalized bivariate (GB) transform are presented. In Section 3, existence and uniqueness of a continuous solution are shown for time fractional K-S, S-H and C-H equations. In Section 4, solution procedure of the proposed algorithms is explained for general non-linear initial value problems. In Section 5, the application of theory developed in the above sections has been presented through several test problems. These are analyzed via comparative and error analysis to test efficacy and robustness of the proposed scheme. In the last section the concluding remarks are presented based on the above study.

Preliminary Results

This section covers the definitions, properties, and terminologies of L-C derivative and GB transform, which are discussed in further detail throughout the paper.

Definition 1. [15] The R-L fractional integral of order α is conceptualized as

$$I_{\eta}^{\alpha} w(\eta) = \begin{cases} \frac{1}{\Gamma(\alpha)} \int_0^{\eta} (\eta - \tau)^{\alpha - 1} w(\eta) d\tau; & \alpha > 0, \eta > 0, \\ w(\eta); & \alpha = 0. \end{cases} \quad (6)$$

Definition 2. [15] For a given function $w(\eta)$: $[0,\infty) \to R$, the L-C fractional derivative of w of order $n\text{-}1 < \alpha \leq n$ is defined by

$$C_{\eta}^{\alpha} w(\eta) = \frac{\partial^{\alpha} w}{\partial \eta^{\alpha}} = \begin{cases} \frac{1}{\Gamma(n-\alpha)} \int_0^{\eta} (\eta - \zeta)^{n-\alpha-1} \frac{\partial^n}{\partial \eta^n} w(\zeta) \mathrm{d}\zeta; & n-1 < \alpha < n, \\ \frac{\partial^n}{\partial \eta^n} w(\eta); & \alpha = n \in N. \end{cases} \quad (7)$$

Lemma 1. [15] For any $n\text{-}1 < \alpha \leq n$, $n \in N$. Then one hass

$$I_{\eta}^{\alpha} C_{\eta}^{\alpha} w(\eta) = w(\eta) - \sum_{k=0}^{n-1} w^{(k)}(0) \frac{\eta^k}{k!}. \quad (8)$$

In the subsequent development of fractional calculus, the operational features of integral transforms are extensively explored to construct solutions to fractional models [4,49,50,61]. However, each existing integral transform pursues some constraints, which stimulates interest in developing modified integral transforms.

In this series of developments, a large amount of research work has been devoted to formulate several novel integral

transforms [62-70]. In 2023, Arora et al. [70] proposed GB transform as the generalization of Laplace, Shehu, ARA and Formable transforms [63,64,68]. Mathematically, the GB transform of order m and its inverse can be defined as [70]:

$$\mathbb{A}_m[w(\eta)] = \mathcal{V}_m(s,\gamma) = \frac{s}{\gamma}\int_0^\infty \eta^{m-1} e^{\frac{-s}{\gamma}\eta} w(\eta)\, d\eta, \tag{9}$$

and

$$\mathbb{A}_m^{-1}[\mathcal{V}_m(s,\gamma)] = w(\eta) = \frac{(-1)^{2(m-1)}}{2\pi i}\int_{\delta-i\infty}^{\delta+i\infty} \frac{1}{\gamma} e^{\frac{s}{\gamma}\eta} \mathbb{S}(s,\gamma)\, ds, \tag{10}$$

over the set of functions

$$\mathcal{S} = \{w(\eta): \exists\, B, b_j > 0, |w(\eta)| < Be^{\frac{|\eta|}{b_j}},$$
$$i!\, f\ \eta \in (-1)^j \times [0,\infty)\ for\ j = 1,2\},$$

where $s > \gamma > 0$, δ is real constant and $\mathbb{S}$ is the Shehu transform [68].

Proposition 1. [70] GB transform holds the fundamental properties of integral transforms such as:

- Linearity Property

$$\mathbb{A}_m[\mu u(\eta) + \lambda w(\eta)] = \mu \mathbb{A}_m[u(\eta)] + \lambda \mathbb{A}_m[w(\eta)]. \tag{11}$$

- Convolution Property

$$\mathbb{A}_1[(u * w)(\eta)] = \frac{s}{\gamma}\mathbb{A}_1[u(\eta)].\mathbb{A}_1[w(\eta)]. \tag{12}$$

- Derivative Property

$$\mathbb{A}_m[w^n(\eta)] = (-1)^{m-1}\frac{s}{\gamma}\frac{\partial^{m-1}}{\partial s^{m-1}}\left[\left(\frac{s}{\gamma}\right)^{n-1}\mathbb{A}_1[w(\eta)] - \sum_{k=0}^{n-1}\left(\frac{s}{\gamma}\right)^{n-(k+1)} w^k(0)\right], \tag{13}$$

where μ and λ are arbitrary constants.

Theorem 1. [71] Formulation for application of GB transform over L-C derivative is given by

$$\mathbb{A}_m\left[{}_0^C C_\eta^\alpha(w(\eta))\right] = \frac{1}{\Gamma(n-\alpha)}\sum_{r=1}^m \binom{m-1}{r-1}\Gamma(n+m-\alpha-r)\frac{\gamma^{n-\alpha}}{s^{n+m-\alpha-r}}\mathbb{A}_r[w^n(\eta)], \tag{14}$$

where $n\text{-}1 < \alpha \le n$

Existence and Uniqueness

The present section illustrates the existence and uniqueness of continuous solutions for the considered fractional equations.

The FGKS reads as:

$$C_\eta^\alpha w = -ww_\xi - xw_{\xi\xi} - yw_{\xi\xi\xi} - zw_{\xi\xi\xi\xi\xi}. \tag{15}$$

Employing the fractional integral operator given in Equation 6 on Equation 15, gives

$$w(\xi,\eta) - w(\xi,0) = I_\eta^\alpha\left(-ww_\xi - xw_{\xi\xi} - yw_{\xi\xi\xi} - zw_{\xi\xi\xi\xi\xi}\right),$$

or explicitly

$$w(\xi,\eta) - w(\xi,0) = \frac{1}{\Gamma(\alpha)}\int_0^\eta (\eta-\tau)^{\alpha-1}\left(-ww_\xi - xw_{\xi\xi} - yw_{\xi\xi\xi} - zw_{\xi\xi\xi\xi\xi}\right)d\tau. \tag{16}$$

Let

$$N(\xi,\eta,w,x,y,z) := -ww_\xi - xw_{\xi\xi} - yw_{\xi\xi\xi} - zw_{\xi\xi\xi\xi\xi}.$$

In the same manner one can define

- For FSH equation:

$$N(\xi,\eta,w,x,y,z) := w_{\xi\xi\xi\xi} - 2w_{\xi\xi} + xw_{\xi\xi\xi} + yw + 2w^2 - w^3. \tag{17}$$

- For FCH equation:

$$N(\xi,\eta,w,x,y,z) := ww_\xi + \left(-w_{\xi\xi} - w + w^3\right)_{\xi\xi}. \tag{18}$$

Lemma 2. [72] The function N satisfies the Lipschitz condition.

Proof: Let w and w^* be two bounded functions. Using definition of N and triangular inequality gives

$$\begin{aligned} &\| N(\xi,\eta,w,x,y,z) - N(\xi,\eta,w^*,x,y,z)\\ &\| \le \| ww_\xi - w^*w_\xi^* \| + x \| (w-w^*)_{\xi\xi}\\ &\| + y \| (w-w^*)_{\xi\xi\xi} \| + z \| (w-w^*)_{\xi\xi\xi\xi},\\ &= \frac{1}{2}\| (w^2-w^{*2})_\xi \| + x \| (w-w^*)_{\xi\xi}\\ &\| + y \| (w-w^*)_{\xi\xi\xi} \| + z \| (w-w^*)_{\xi\xi\xi\xi} \|. \end{aligned}$$

Now suppose that $\exists$ constants $\kappa_1, \kappa_2 > 0$ such that $\forall(\xi,\eta)$ $\|w\| \le \kappa_1$ and $\|w^*\| \le \kappa_2$. $\kappa = \max\{\kappa_1, \kappa_2\}$.

Then their first derivative function $(.)_\xi$ fulfills Lipschitz condition and $\exists$ a non-negative number L_1 such that

$$\begin{aligned} &\le \frac{1}{2}L_1 \| (w^2-w^{*2}) \| + xL_1^2 \| (w-w^*) \| + yL_1^3\\ &\| (w-w^*)_{\xi\xi\xi} \| + zL_1^4 \| (w-w^*) \|,\\ &\le (\kappa L_1 + xL_1^2 + yL_1^3 + zL_1^4) \| w-w^* \|, \end{aligned} \tag{19}$$

where $\| w^2\text{-}w^{*2}\| < 2\kappa \| w\text{-}w^*\|$. Hence,

$$\| N(\xi,\eta,w,x,y,z) - N(\xi,\eta,w^*,x,y,z) \| \le L \| w\text{-}w^* \|,$$

where

$$L := \kappa L_1 + xL_1^2 + yL_1^3 + zL_1^4.$$

In the same manner one can deduce

- For FSH equation

$$L := L_1^4 + 2L_1^2 + xL_1^3 + y + 4\kappa + 4\kappa^2. \tag{20}$$

- For FCH equation

$$L := xL_1 + L_1^4 + L_1^2 + 4\kappa^2 L_1^2, \tag{21}$$

where $\| w^3\text{-}w^{*3} \| \le 4\kappa^2 \| w\text{-}w^* \|$.

Theorem 2. [72] The FGKS, FSH and FCH equations admit a unique continuous solution provided that $\frac{L}{\Gamma(\alpha+1)}\eta^{\alpha} < 1$.

Proof: The expressions 16, 17 and 18 can be expressed in a unified form as

$$w(\xi,\eta) - w(\xi,0) = \frac{1}{\Gamma(\alpha)}\int_0^{\eta}(\eta-\tau)^{\alpha-1} N(\xi,\eta,w,x,y,z)d\tau, \quad (22)$$

which recommends the consideration of recurrence relation as

- $w_0(\xi,\eta) = w(\xi,0)$,
- $w_{\mathrm{k}}(\xi,\eta) = \frac{1}{\Gamma(\alpha)}\int_0^{\eta}(\eta-\tau)^{\alpha}\,\mathrm{N}(\xi,\eta,w_{k-1},\mathrm{x},\mathrm{y},\mathrm{z})\mathrm{d}\tau$.

Let

$$\overline{w}(\xi,\eta) = \lim_{k\to\infty} w_k(\xi,\eta). \quad (23)$$

Now the aim is to prove that $\overline{w}(\xi,\eta) = w(\xi,\eta)$ is a continuous solution. For that end, set the algebraic difference of successive terms as

$$\Theta_k(\xi,\eta) = w_k(\xi,\eta) - w_{k-1}(\xi,\eta).$$

Note that

$$w_k(\xi,\eta) = \sum_{i=0}^{k}\Theta_i(\xi,\eta).$$

It is easy to observe that

$$\|\Theta_k(\xi,\eta)\| = \|w_k(\xi,\eta) - w_{k-1}\| \le \frac{1}{\Gamma(\alpha)}\int_0^{\eta}(\eta-\tau)^{\alpha-1}$$
$$\|N(\xi,\eta,w_{k-1},x,y,z)N(\xi,\eta,w_{k-2},x,y,z)\|d\tau.$$

Lipschitz condition for N yields

$$\|\Theta_k(\xi,\eta)\| \le \frac{1}{\Gamma(\alpha)}\int_0^{\eta}(\eta-\tau)^{\alpha-1}\|w_{k-1} - w_{k-2}\|d\tau,$$
$$\le \frac{L}{\Gamma(\alpha)}\int_0^{\eta}(\eta-\tau)^{\alpha-1}\|\Theta_{k-1}(\xi,\eta)\|d\tau. \quad (24)$$

Following the recurrence procedure given in Equation 24 deduce

$$\|\Theta_k(\xi,\eta)\| \le \left(\frac{\eta^{\alpha}L}{\Gamma(\alpha+1)}\right)^{k}\|w(\xi,0)\|,$$

which implies the existence and continuity of the solution.

Now to prove that $w(\xi,\eta) = \lim_{k\to\infty} w_k(\xi,\eta)$ is the solution of the Cauchy problems defined as FKS, FSH and FCH equations. Let

$$\Psi_k(\xi,\eta) = \overline{w} - w_k(\xi,\eta),\ k \in N.$$

Thus,

$$\overline{w} - w_{k+1} = \frac{1}{\Gamma(\alpha)}\int_0^{\eta}(\eta-\tau)^{\alpha-1}[N(\xi,\eta,\overline{w},x,y,z) - N(\xi,\eta,w_k,x,y,z)]d\tau.$$

Lipschitz condition for N yields

$$\|\overline{w}(\xi,\eta) - w_{k+1}\| \le \frac{L}{\Gamma(\alpha)}\int_0^{\eta}(\eta-\tau)^{\alpha-1}\|\overline{w} - w_k\|d\tau,$$
$$= \frac{L\eta^{\alpha}}{\Gamma(\alpha+1)}\|\Psi_k(\xi,\eta)\|. \quad (25)$$

Evaluating the limit $k \to \infty$ for Equation 25 yields $\Psi_k \to 0$ and left-hand side gives

$$\lim_{k\to\infty} w_k = \overline{w}.$$

The above result implies the certainty of taking $\overline{w}(\xi,\eta) = w(\xi,\eta)$ as a solution which is continuous. Finally for uniqueness consider w and $w^{\star}$ be two distinct solutions for FKS, FSH and FCH equations then Equation 24 and Lipschitz condition of N implies

$$\|w - w^{*}\| \le \frac{L\eta^{\alpha}}{\Gamma(\alpha+1)}\|w - w^{*}\|,$$

or equivalently

$$\|w - w^{*}\|\left(1 - \frac{L\eta^{\alpha}}{\Gamma(\alpha+1)}\right) \le 0.$$

Hence, $w = w^{\star}$ if $\left(\frac{L\eta^{\alpha}}{\Gamma(\alpha+1)}\right) < 1$. The theorem is proved.

Application of Generalized Bivariate Homotopy Perturbation Method

In this section, the fundamental idea behind the solution procedure of the proposed algorithms is elucidated. The general form of the fractional non-linear partial differential equation can be considered as:

$$C_{\eta}^{\alpha}w(\xi,\eta) = \mathcal{P}[w(\xi,\eta)] + \mathcal{Q}[w(\xi,\eta)] + \mathcal{N}(\xi,\eta); \xi \in \Omega \subset R^{n}, \eta \in [0,T], \quad (26)$$

subject to the initial condition

$$w(\xi,0) = h(\xi), \quad (27)$$

where w is the function of ξ and η. Ω is a bounded domain and T is finite time. $\mathcal{P}$ and $\mathcal{Q}$ are linear and non-linear operators, respectively, and $N(\xi,\eta)$ is the non-homogeneous term.

Apply A_1 on both sides of Equation 26 and use initial condition given in Equation 27, such that Equation 26 takes the following form:

$$\mathbb{A}_1[w(\xi,\eta)] = h(\xi) + \left(\frac{\gamma}{s}\right)^{\alpha}\mathbb{A}_1[\mathcal{N}(\xi,\eta)] + \left(\frac{\gamma}{s}\right)^{\alpha}\mathbb{A}_1\{\mathcal{P}[w(\xi,\eta)] + \mathcal{Q}[w(\xi,\eta)]\}. \quad (28)$$

Operating $\mathbb{A}_1^{-1}$ to Equation 28, yields

$$w(\xi,\eta) = h(\xi) + \mathbb{A}_1^{-1}\left\{\left(\frac{\gamma}{s}\right)^{\alpha}\mathbb{A}_1[\mathcal{N}(\xi,\eta)]\right\} + \mathbb{A}_1^{-1}\left\{\left(\frac{\gamma}{s}\right)^{\alpha}\mathbb{A}_1\{\mathcal{P}[w(\xi,\eta)] + \mathcal{Q}[w(\xi,\eta)]\}\right\}, \quad (29)$$
$$= \mathcal{G}(\xi,\eta) + \mathbb{A}_1^{-1}\left\{\left(\frac{\gamma}{s}\right)^{\alpha}\mathbb{A}_1\{\mathcal{P}[w(\xi,\eta)] + \mathcal{Q}[w(\xi,\eta)]\}\right\},$$

which is a recurrence relation for Equation 26, where $\mathcal{G}(\xi,\eta)$ denotes the term that arises from the non-homogeneous term and initial condition.

Here, it is worth noting that for existing integral transforms $\mathcal{I}[f.g] \neq \mathcal{I}[f].\mathcal{I}[g]$ where, $\mathcal{I}$ is an integral transform. Therefore, these integral transforms are insufficient for handling a large class of differential and integral equations due to the restrictions arising from non-linear terms. In the present scheme, GB transform is consolidated with homotopy perturbation method (HPM) [73] to overlap this difficulty.

According to the expansion methodology, which is followed by semi-analytic tools, let the solution be represented by the following infinite series:

$$w(\xi,\eta) = \sum_{k=0}^{\infty}\theta^k w_k(\xi,\eta). \quad (30)$$

Homotopy is a continuous process that associates a family of objects, which represent intermediatory stages of deformation of an object to another object. HPM is a semi-analytic strategy that relies on the principles of homotopy and perturbation methods. Application of HPM redistributes the existing non-linearities with the aid of homotopy parameter i.e., θ. The smooth tracing of homotopy parameter θ in [0,1] is equivalent to the variance in the strength of inherited non-linearity. This enhances to deform an accessible solution into the desired one.

To consolidate the limitations of GB transform for non-linear events, HPM offers the decomposition of non-linear terms such as:

$$\mathcal{Q}[w(\xi,\eta)] = \sum_{k=0}^{\infty}\theta^k\mathcal{H}_k = \mathcal{H}_0 + \theta\mathcal{H}_1 + \theta^2\mathcal{H}_2 + \theta^3\mathcal{H}_3 + \cdots, \quad (31)$$

where $\mathcal{H}_{\hbar}$ are considered to be the He's polynomials [74], given by

$$\mathcal{H}_k(w_0, w_1, w_2, \ldots, w_n) = \frac{1}{k!}\frac{\partial^k}{\partial\theta^k}\left[\mathcal{Q}\left(\sum_{k=0}^{\infty}\theta^k w_k\right)\right].$$

Using Equation 30 and Equation 31 in Equation 29 parametric homotopy equation with homotopy parameter θ can be constructed as

$$\sum_{k=0}^{\infty}\theta^k w_k(\xi,\eta) = \mathcal{G}(\xi,\eta) + \theta\left\{\mathbb{A}_1^{-1}\left[\left(\frac{\gamma}{s}\right)^{\alpha}\mathbb{A}_1\left(\mathcal{P}\left[\sum_{k=0}^{\infty}\theta^k w_k(\xi,\eta)\right] + \sum_{k=0}^{\infty}\theta^k\mathcal{H}_k\right)\right]\right\}.$$

Comparing the coefficients of like powers of homotopy parameter i.e., θ, derives

$$\theta^0: w_0(\xi,\eta) = \mathcal{G}(\xi,\eta),$$
$$\theta^1: w_1(\xi,\eta) = \mathbb{A}_1^{-1}\left[\left(\frac{\gamma}{s}\right)^{\alpha}\mathbb{A}_1(\mathcal{P}[w_0] + \mathcal{H}_0)\right],$$
$$\theta^2: w_2(\xi,\eta) = A_1^{-1}\left[\left(\frac{\gamma}{s}\right)^{\alpha}\mathbb{A}_1(\mathcal{P}[w_1] + \mathcal{H}_1)\right],$$
$$\vdots$$
$$\theta^k: w_k(\xi,\eta) = \mathbb{A}_1^{-1}\left[\left(\frac{\gamma}{s}\right)^{\alpha}\mathbb{A}_1(\mathcal{P}[w_{k-1}] + \mathcal{H}_{\hbar-1})\right].$$

The approximate solution of n^{th}-order for the Equation 26 can be obtained as:

$$W_n = \lim_{\theta\to 1}\sum_{k=0}^{n}\theta^k w_k = \sum_{k=0}^{n} w_k. \quad (32)$$

Test Problems

This section is devoted to extracting and discussing the semi-analytic results of the L-C fractional FGKS, FSH and FCH equations under various initial conditions. The comparative analysis of the proposed algorithms is developed using graphical and tabular representations of the results.

Example 1. Consider FGKS without dispersion effect at $x = -1$, $y = 0$ and $z = 1$ for which initial condition is extracted from the analytic solution:

$$w(\xi,\eta) = s + \frac{15tanh^3(\kappa(\xi - s\eta - \lambda)) - 45tanh(\kappa(\xi - s\eta - \lambda))}{19\sqrt{19}}, \quad (33)$$

where s, κ and λ are real constants.

The computational work carried out with choice of

$$\mathcal{P}[w(\xi,\eta)] = -\left(xw_{\xi\xi} + zw_{\xi\xi\xi\xi}\right),$$
$$\mathcal{Q}[w(\xi,\eta)] = -ww_{\xi}, \text{ and } \mathcal{N}(\xi,\eta) = 0,$$

produces components of the series solutions in terms of GB-HPM solution as

$$w_0(\xi,\eta) = s + \left(\sqrt{19}\left(45tanh(\kappa(\lambda-\xi)) - 15tanh(\kappa(\lambda-\xi))^3\right)\right)/361$$
$$w_1(\xi,\eta) = \left(45\sqrt{19}\kappa\eta^{\alpha}\left(tanh(\kappa(\lambda-\xi)) - 1\right)^2\left(tanh(\kappa(\lambda-\xi)) + 1\right)^2\left(361s - 15\sqrt{19}tanh(\kappa(\lambda-\xi))^3 20216\kappa^3 tanh(\kappa(\lambda\xi)) + 43320\kappa^3 tanh(\kappa(\lambda-\xi))^3 + 45\sqrt{19}tanh(\kappa(\lambda-\xi)) - 1444\kappa tanh(\kappa(\lambda-\xi))\right)\right)/\left(130321\Gamma(\alpha+1)\right)\ldots.$$

The solution profile of GB-HPM solution at $s = 5, \lambda = -25, \kappa = \frac{1}{2\sqrt{19}}$ is drawn in Figure 1 and Figure 2. These graphs represent the behavior for integer order K-S equation with $\alpha = 1$ and the variation arises for different values of α in 3D and contour surfaces. The sensitivity of GB-HPM solution profiles with respect to the time

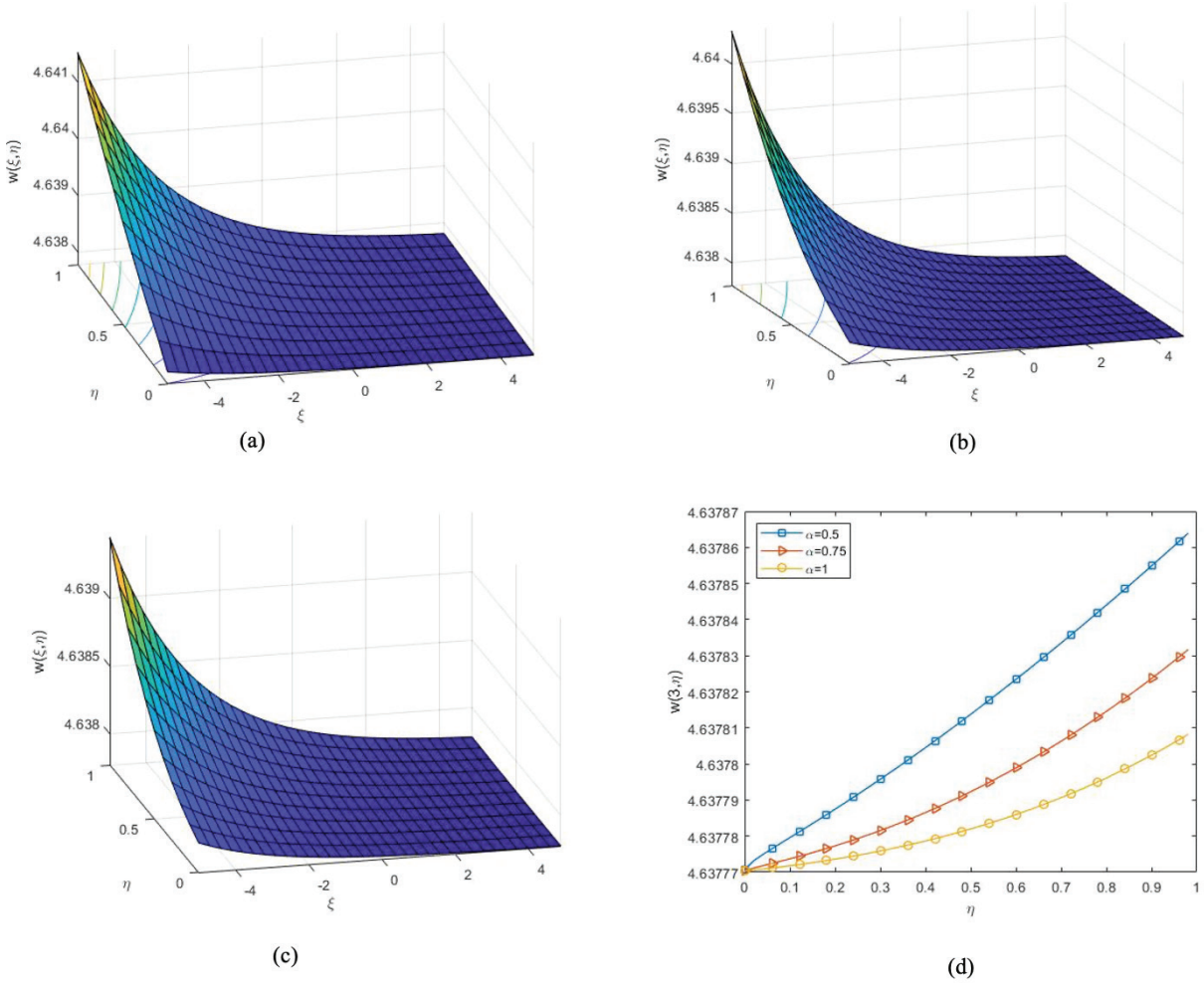

Figure 1. Solution profile of GB-HPM solution for Example 1 when (a) $\alpha = 0.5$ (b) $\alpha = 0.75$ (c) $\alpha = 1$ (d) $\xi = 3$.

fractional orders can be observed apparently through 2D simulations given in Figure 1(d) at $\xi = 3$ and contour surfaces in Figure 2. Fractional solution profile converges to the solution of integer order equation as $\alpha \to 1$. 3D surface plots of FGKS exhibit time evolution of flame-front. The contour surfaces effectively highlight the patterns in the data which reflects the heat distribution in the system. The fractional derivative reveals broader visualization of evolutionary process with its enhancing feature of controlling rate of change.

Table 1 shows the numerical findings for different time fractional orders. The absolute error is found competent and aligned to the error deduced for q-HATM scheme [24]. However, the present scheme is free from analysis of any auxiliary parameter. Table 2 demonstrates the convergence phenomenon of series solution for fractional derivative $\alpha = 0.75$. It provides the credibility of obtained solution for fractional phenomenon when exact solution is unknown. The convergence rate gets slower as time increases.

Example 2. Consider the FGKS equation with dispersion effect at $x = 1$, $y = 4$, and $z = 1$. The analytic solution is given by

$$w(\xi,\eta) = s + 9 - 15[tanh(\theta) + tanh^2(\theta) - tanh^3(\theta)], \quad (34)$$

where $\theta = \kappa(\xi - s\eta - s_0)$ with arbitrary constant s and s_0.

With choice of

$$\mathcal{P}[w(\xi,\eta)] = -\left(xw_{\xi\xi} + yw_{\xi\xi\xi} + zw_{\xi\xi\xi\xi}\right),$$
$$\mathcal{Q}[w(\xi,\eta)] = ww_{\xi}, \text{ and } \mathcal{N}(\xi,\eta) = 0,$$

and using the initial conditions from Equation 34 at $\eta = 0$, the suggested algorithm gives the explicit expressions of components of series solutions in terms of GB-HPM solution as

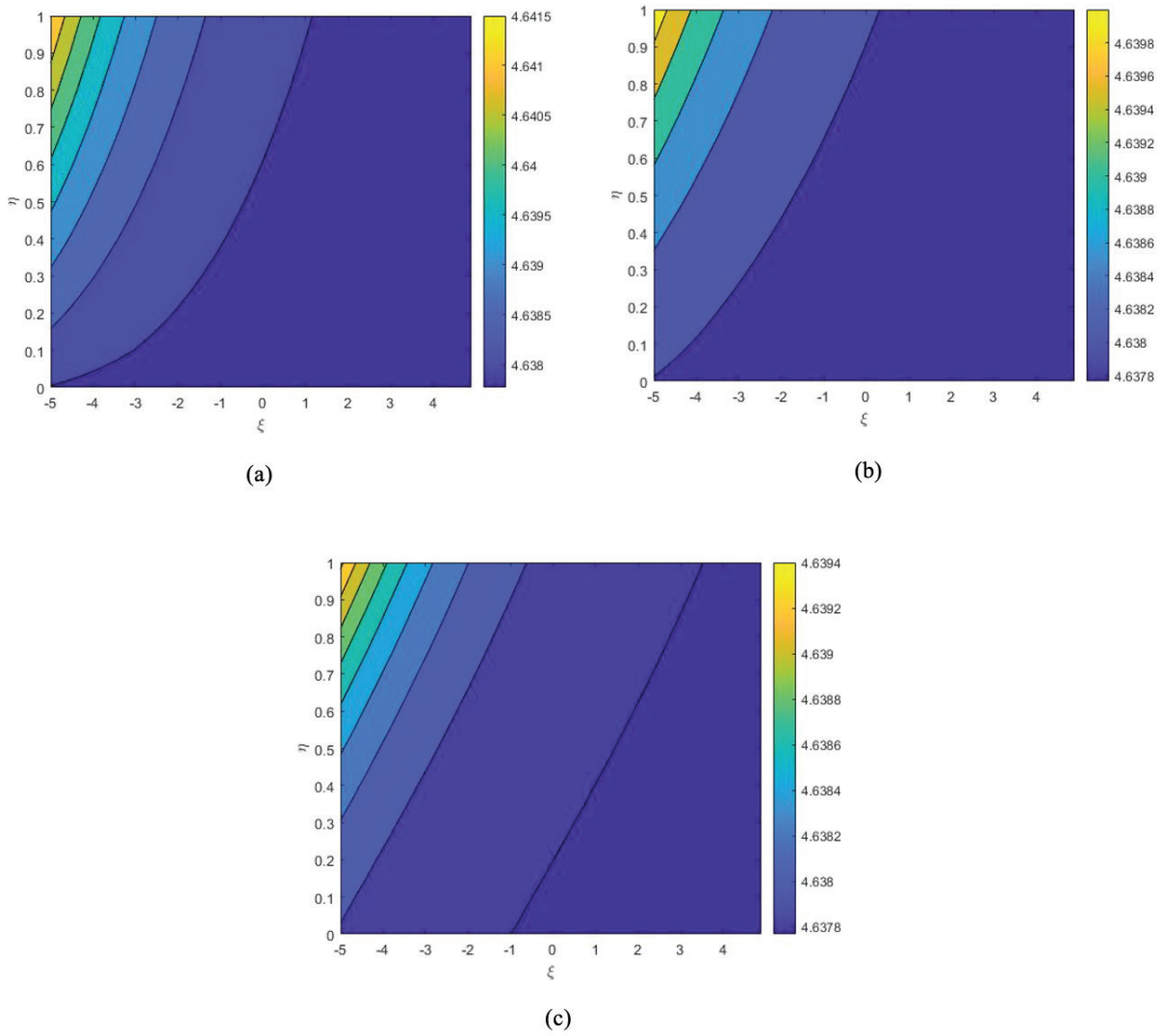

Figure 2. Contour surfaces of GB-HPM solution for Example 1when (a) $\alpha = 0.5$ (b) $\alpha = 0.75$ (c) $\alpha = 1$.

$$w_0(\xi,\eta) = s + 15tanh\big(\kappa(s_0-\xi)\big) - 15tanh\big(\kappa(s_0-\xi)\big)^2 - 15tanh\big(\kappa(s_0-\xi)\big)^3 + 9,$$

$$w_1(\xi,\eta) = -\Big(15\kappa\eta^{\alpha}\big(tanh\big(\kappa(s_0-\xi)\big)-1\big)\big(tanh\big(\kappa(s_0-\xi)\big)+1\big)^2\big(s+2\kappa-12tanh\big(\kappa(s_0-\xi)\big) - 12\kappa tanh\big(\kappa(s_0-\xi)\big)^2 + 96\kappa^2 tanh\big(\kappa(s_0-\xi)\big) - 120\kappa^3 tanh\big(\kappa(s_0-\xi)\big) - 60tanh\big(\kappa(s_0-\xi)\big)^2 + 30tanh\big(\kappa(s_0-\xi)\big)^3 + 45tanh\big(\kappa(s_0-\xi)\big)^4 + 144\kappa^2 tanh\big(\kappa(s_0-\xi)\big)^2 - 240\kappa^2 tanh\big(\kappa(s_0-\xi)\big)^3 + 240\kappa^3 tanh\big(\kappa(s_0-\xi)\big)^2 + 240\kappa^3 tanh\big(\kappa(s_0-\xi)\big)^3 - 360\kappa^3 tanh\big(\kappa(s_0-\xi)\big)^4 - 3stanh\big(\kappa(s_0-\xi)\big) + 6\kappa tanh\big(\kappa(s_0-\xi)\big) - 32\kappa^2 - 16\kappa^3 + 9\big)\Big)/\Gamma(\alpha+1),$$

and so on. For parameters $s = 3$, $\kappa = 0.5$ and $s_0 = -13$, Figure 3 and Figure 4 exhibit the dynamics that have been produced by the explicit expression of GB-HPM solution for Example 2. To visualize the variability in solution profile in temporal domain at $\xi = 3$, 2D solution profiles are drawn in Figure 3(d) for different values of α. Figure 4 simulates the projection of solution profile for distinct orders of fractional derivative. In this case of incorporating dispersion effect the flame-fronts exhibit some sharpness. The contour surfaces strikingly illustrate the regions of sharp transitions or abrupt changes which implies the occurring of steep thermal gradient.

Numerical values of the GB-HPM solution for severe fractional orders are tabulated in Table 3. In addition, error analysis in terms of absolute error of proposed solutions in comparison to q-HATM [24] reveals the supremacy of GB-HPM. This performance of accomplished results for FGKS equation with dispersion ensures the capability of the present method to capture every comprised effect of the system.

Table 1. Absolute error for approximate solution of Example 1 at $\kappa = 1/(2\sqrt{19})$, $s = 5$, $\lambda = -25$ for different α

ξ	η	$\alpha = 0.75$		$\alpha = 1$	
		GB-HPM	**q-HATM [24]**	**GB-HPM**	**q-HATM [24]**
1	0.2	9.11157×10^{-6}	9.11157×10^{-6}	2.80432×10^{-8}	2.80432×10^{-8}
	0.4	1.91218×10^{-5}	1.91218×10^{-5}	4.95160×10^{-7}	4.95160×10^{-7}
	0.6	2.93491×10^{-5}	2.93491×10^{-5}	2.78309×10^{-6}	2.78309×10^{-6}
	0.8	3.60085×10^{-5}	3.60085×10^{-5}	9.82802×10^{-6}	9.82802×10^{-6}
	1	3.27450×10^{-5}	3.27450×10^{-5}	2.69893×10^{-5}	2.69893×10^{-5}
2	0.2	5.77566×10^{-6}	5.77566×10^{-6}	1.78573×10^{-8}	1.78573×10^{-8}
	0.4	1.21255×10^{-5}	1.21255×10^{-5}	3.15448×10^{-7}	3.15448×10^{-7}
	0.6	1.86103×10^{-5}	1.86103×10^{-5}	1.77397×10^{-6}	1.77397×10^{-6}
	0.8	2.28157×10^{-5}	2.28157×10^{-5}	6.26876×10^{-6}	6.26876×10^{-6}
	1	2.06795×10^{-5}	2.06795×10^{-5}	1.72296×10^{-5}	1.72296×10^{-5}
3	0.2	3.65888×10^{-6}	3.65888×10^{-6}	1.13536×10^{-8}	1.13536×10^{-8}
	0.4	7.68382×10^{-6}	7.68382×10^{-6}	2.00632×10^{-7}	2.00632×10^{-7}
	0.6	1.17929×10^{-5}	1.17929×10^{-5}	1.12878×10^{-6}	1.12878×10^{-6}
	0.8	1.44489×10^{-5}	1.44489×10^{-5}	3.99096×10^{-6}	3.99096×10^{-6}
	1	1.30614×10^{-5}	1.30614×10^{-5}	1.09765×10^{-5}	1.09765×10^{-5}
4	0.2	2.31680×10^{-6}	2.31680×10^{-6}	7.20976×10^{-9}	7.20976×10^{-9}
	0.4	4.86653×10^{-6}	4.86653×10^{-6}	1.27441×10^{-7}	1.27441×10^{-7}
	0.6	7.46887×10^{-6}	7.46887×10^{-6}	7.17246×10^{-7}	7.17246×10^{-7}
	0.8	9.14654×10^{-6}	9.14654×10^{-6}	2.53702×10^{-6}	2.53702×10^{-6}
	1	8.25068×10^{-6}	8.25068×10^{-6}	6.98138×10^{-6}	6.98138×10^{-6}

Table 2. Absolute error in consecutive approximate solutions of Example 1 at $\kappa = 1/(2\sqrt{19})$, $s = 5$, $\lambda = -25$ for $\alpha = 0.7$

ξ	η	$\lvert W_2 - W_1 \rvert$	$\lvert W_3 - W_2 \rvert$	$\lvert W_4 - W_3 \rvert$
-5	0.01	8.37493×10^{-7}	3.07223×10^{-8}	9.03484×10^{-10}
	0.1	2.64839×10^{-5}	5.46328×10^{-6}	9.03484×10^{-7}
	0.5	2.96099×10^{-4}	2.04238×10^{-4}	1.12936×10^{-4}
-1	0.01	1.38596×10^{-7}	5.17944×10^{-9}	1.56727×10^{-10}
	0.1	4.38278×10^{-6}	9.21050×10^{-7}	1.56727×10^{-7}
	0.5	4.90010×10^{-5}	3.44323×10^{-5}	1.95909×10^{-5}
1	0.01	5.58599×10^{-8}	2.09697×10^{-9}	6.38892×10^{-11}
	0.1	1.76645×10^{-6}	3.72901×10^{-7}	6.38892×10^{-8}
	0.5	1.97495×10^{-5}	1.39404×10^{-5}	7.98615×10^{-6}
5	0.01	8.99584×10^{-9}	3.39273×10^{-10}	1.04094×10^{-11}
	0.1	2.84473×10^{-7}	6.03323×10^{-8}	1.04094×10^{-8}
	0.5	3.18051×10^{-6}	2.25545×10^{-6}	1.30118×10^{-6}

Example 3. Consider FSH equation without dispersion effect with initial data

$$w(\xi, 0) = \frac{1}{10} sin\left(\frac{\pi\xi}{l}\right), \tag{35}$$

where l is a real constant.

Following the computational procedure of GB-HPM with choice of

$$\mathcal{P}[w(\xi,\eta)] = -w_{\xi\xi\xi\xi} - 2w_{\xi\xi} - (1-x)w,$$
$$\mathcal{Q}[w(\xi,\eta)] = -w^3, \text{ and } \mathcal{N}(\xi,\eta) = 0,$$

yields the components of expansion solutions as

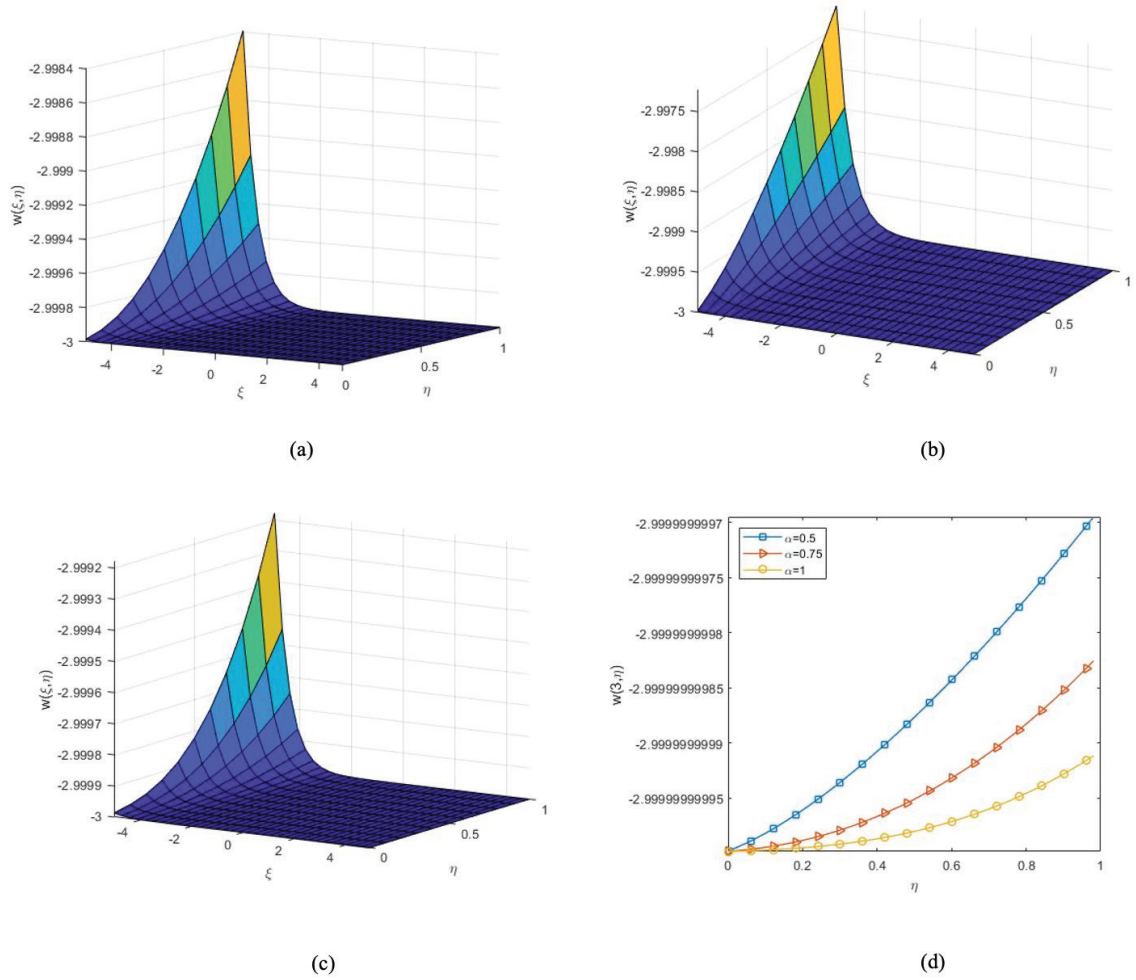

Figure 3. Solution profile of GB-HPM solution for Example 2 when (a) (a) $\alpha = 0.5$ (b) $\alpha = 0.75$ (c) $\alpha = 1$ (d) $\xi = 3$.

$$w_0(\xi,\eta) = sin\left((\pi\xi)/l\right)/10,$$

$$w_1(\xi,\eta) = \frac{-\left(\eta^{\alpha} sin\left((\pi\xi)/l\right)\left(100\pi^4 - 100\xi l^4 + 100l^4 - 200l^2\pi^2 + l^4 sin\left((\pi\xi)/l\right)^2\right)\right)}{\left(1000l^4\Gamma(\alpha+1)\right)},$$

$$\begin{aligned} w_2(\xi,\eta) = \frac{1}{\left(100000l^8\Gamma(2\alpha+1)\right)}\Big(&\eta^{2\alpha} sin\left((\pi\xi)/l\right)\Big(10000\pi^8 - 20000\xi l^8 \\ &+ 10000l^8 - 40000l^2\pi^6 + 54000l^4\pi^4 - 38800l^6\pi^2 + 10000\xi^2 l^8 \\ &+ 400l^8 sin\left((\pi\xi)/l\right)^2 + 3l^8 sin\left((\pi\xi)/l\right)^4 - 20000\xi l^4\pi^4 \\ &+ 40000\xi l^6\pi^2 - 400\xi l^8 sin\left((\pi\xi)/l\right)^2 + 8400l^4\pi^4 sin\left((\pi\xi)/l\right)^2 \\ &- 2400l^6\pi^2 sin\left((\pi\xi)/l\right)^2\Big)\Big), \end{aligned}$$

and so on. Solution profile of S-H equation signifies the physical effect of bifurcation and dispersive parameters on probability density function $w(\xi,\eta)$ for fractional Brownian and standard motions. For non-dispersive FSH equation, the graphical representation of GB-HPM solution in Figure 5, Figure 6 and Figure 7 simulate oscillatory and periodic solutions depending on the value of l. The behavior of obtained solutions varies harmonically in space and time. The variation of solution profiles at l = 3,6,8,10 for several fractional order displayed as 2D graphs is apparent in Figure 5, Figure 6 and Figure7. Behavior of obtained solution is more sensitive with respect to the α at $l = 3$, but at l = 6,8,10 there are no changes. For $\alpha = x = 0.5$ overshoots observed for probability density function $w(\xi,\eta)$ increase with increase in η for $l = 3$. However, overshoots of $w(\xi,\eta)$ show inverse relation with time η at l = 6,8,10.

Table 4 demonstrates the numerical results of 3^{rd}- order approximation for Example 3 at distinct fractional orders obtained by GB-HPM in comparison on of NTDM [49] and q-HATM [50] scheme. Obtained results are completely aligned with results of NTDM and agrees with q-HATM solution for atleast upto second significant digit. In comparison with NTDM scheme present method with alternative approach of He polynomials, overcomes the demerit of tedious calculations for Adomian polynomials [74]. In Table 5 the decreasing absolute error of consecutive approximate solutions ensures the convergence of the solution for $\alpha = 0.75$. Therefore, credibility GB-HPM solution is independent from the condition of availability of exact solution.

Example 4. Consider FSH equation without dispersion effect with initial data

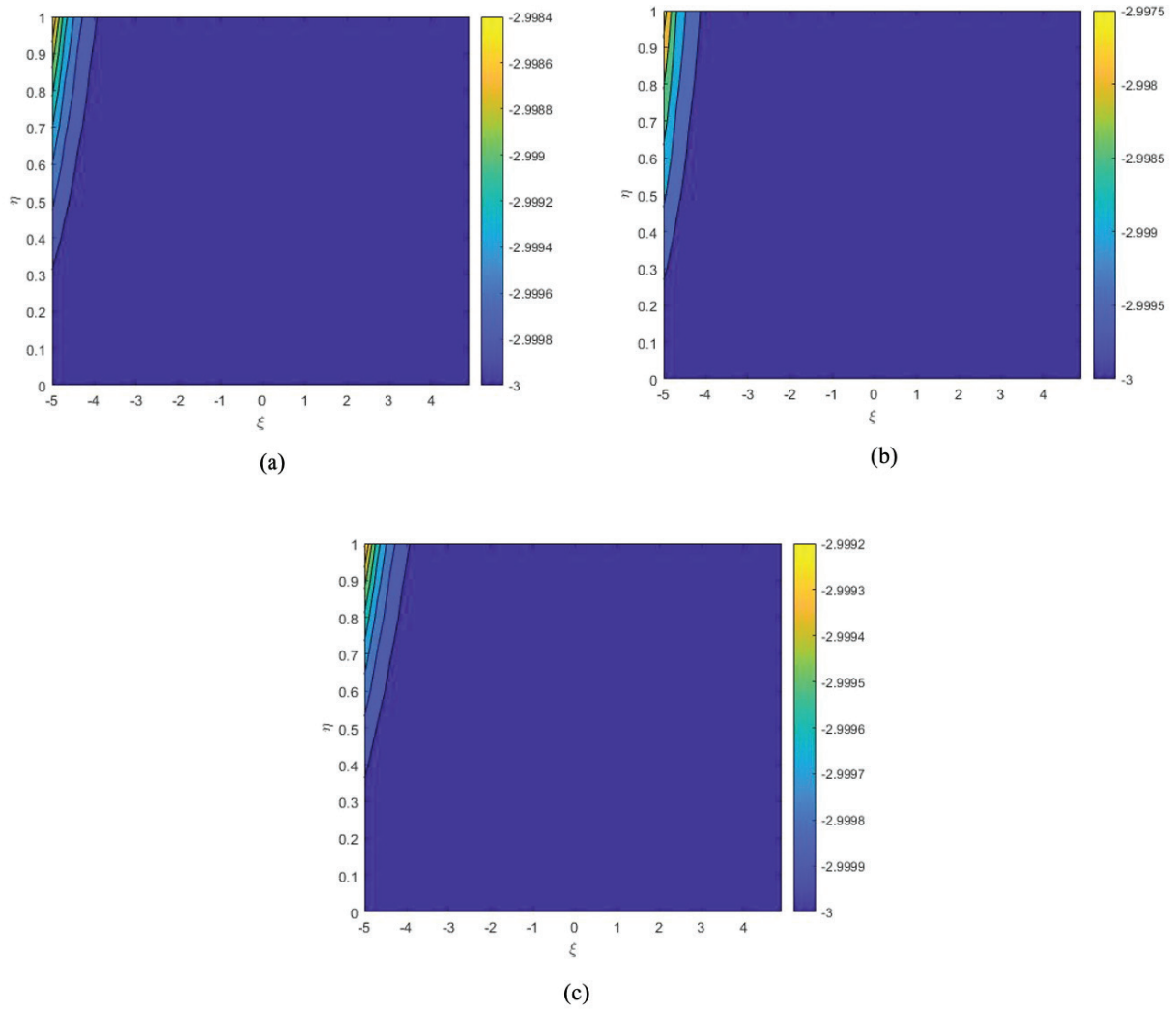

Figure 4. Contour surfaces of GB-HPM solution for Example 2 when (a) $\alpha = 0.5$ (b) $\alpha = 0.75$ (c) $\alpha = 1$.

$$w(\xi,0) = \frac{1}{10}sin\left(\frac{\pi\xi}{l}\right), \tag{36}$$

where l is a real constant.

Following the computational procedure of GB-HPM with choice of

$$\mathcal{P}[w(\xi,\eta)] = -w_{\xi\xi\xi\xi} - 2w_{\xi\xi} + xw_{\xi\xi\xi} + yw,$$
$$\mathcal{Q}[w(\xi,\eta)] = 2w^2 - w^3, \text{ and } \mathcal{N}(\xi,\eta) = 0,$$

yields the components of expansion solutions as

$$w_0(\xi,\eta) = sin\big((\pi\xi)/l\big)/10,$$

$$\begin{aligned} w_1(\xi,\eta) = -\Big(\eta^{\alpha}\Big(&100\pi^4 sin\big((\pi\xi)/l\big) - 20l^4 sin\big((\pi\xi)/l\big)^2 \\ &+ l^4 sin\big((\pi\xi)/l\big)^3 - 200l^2\pi^2 sin\big((\pi\xi)/l\big) \\ &- 100yl^4 sin\big((\pi\xi)/l\big) + 100xl\pi^3 cos\big((\pi\xi)/l\big)\Big)\Big) \\ &/\big(1000l^4\Gamma(\alpha+1)\big), \end{aligned}$$

$$\begin{aligned} w_2(\xi,\eta) = -\Big(\eta^{2\alpha}\Big(&200l^8 cos\big((4\pi\xi)/l\big) - 800l^8 cos\big((2\pi\xi)/l\big) \\ &- 160000\pi^8 sin\big((\pi\xi)/l\big) - 48000yl^8 \\ &- 9630l^8 sin\big((\pi\xi)/l\big) + 3215l^8 sin\big((3\pi\xi)/l\big) \\ &- 3l^8 sin\big((5\pi\xi)/l\big) + 600l^8 + 32000l^4\pi^4 - 64000l^6\pi^2 \\ &- 288000l^4\pi^4 cos\big((2\pi\xi)/l\big) + 192000l^6\pi^2 cos\big((2\pi\xi)/l\big) \\ &+ 640000l^2\pi^6 sin\big((\pi\xi)/l\big) - 644800l^4\pi^4 sin\big((\pi\xi)/l\big) \\ &+ 9600l^6\pi^2 sin\big((\pi\xi)/l\big) + 33600l^4\pi^4 sin\big((3\pi\xi)/l\big) \\ &- 9600l^6\pi^2 sin\big((3\pi\xi)/l\big) - 160000y^2l^8 sin\big((\pi\xi)/l\big) \\ &+ 48000yl^8 cos\big((2\pi\xi)/l\big) + 4800yl^8 sin\big((\pi\xi)/l\big) \\ &- 1600yl^8 sin\big((3\pi\xi)/l\big) + 160000x^2l^2\pi^6 sin\big((\pi\xi)/l\big) \\ &- 320000xl\pi^7 cos\big((\pi\xi)/l\big) + 640000xl^3\pi^5 cos\big((\pi\xi)/l\big) \\ &- 2400xl^5\pi^3 cos\big((\pi\xi)/l\big) + 12000xl^5\pi^3 cos\big((3\pi\xi)/l\big) \\ &+ 320000yl^4\pi^4 sin\big((\pi\xi)/l\big) - 640000yl^6\pi^2 sin\big((\pi\xi)/l\big) \\ &+ 160000xl^5\pi^3 sin\big((2\pi\xi)/l\big) + 320000yxl^5\pi^3 cos\big((\pi\xi)/l\big)\Big)\Big) \\ &/\big(1600000l^8\Gamma(2\alpha+1)\big), \end{aligned}$$

Table 3. Absolute error for approximate solution of Example 2 at $\kappa = 0.5$, s = 3, $s_0 = -13$ for different α

ξ	η	α = 0.75		α = 1	
		GB-HPM	q-HATM [24]	GB-HPM	q-HATM [24]
1	0.2	3.58527×10^{-10}	1.44623×10^{-7}	9.30287×10^{-12}	3.75185×10^{-9}
	0.4	9.03807×10^{-10}	9.87125×10^{-7}	2.02381×10^{-10}	8.16183×10^{-8}
	0.6	6.87414×10^{-10}	1.28593×10^{-6}	1.47209×10^{-9}	5.93605×10^{-7}
	0.8	3.67755×10^{-9}	1.12748×10^{-7}	7.11536×10^{-9}	2.86856×10^{-6}
	1	2.35700×10^{-8}	7.82679×10^{-6}	2.84106×10^{-8}	1.14490×10^{-5}
2	0.2	4.85206×10^{-11}	5.47368×10^{-8}	1.26051×10^{-12}	5.07855×10^{-10}
	0.4	1.22317×10^{-10}	1.33604×10^{-7}	2.73904×10^{-11}	1.10484×10^{-8}
	0.6	9.30283×10^{-11}	1.74032×10^{-7}	1.99230×10^{-10}	3.88396×10^{-7}
	0.8	4.97723×10^{-10}	1.53996×10^{-8}	9.62981×10^{-10}	1.55060×10^{-6}
	1	3.19000×10^{-9}	1.06033×10^{-6}	3.84510×10^{-9}	6.87344×10^{-11}
3	0.2	6.57005×10^{-12}	7.40806×10^{-9}	1.67069×10^{-13}	1.49536×10^{-9}
	0.4	1.65574×10^{-11}	1.80819×10^{-8}	3.70357×10^{-12}	1.08769×10^{-8}
	0.6	1.25933×10^{-11}	2.35527×10^{-8}	2.69595×10^{-11}	5.25725×10^{-8}
	0.8	6.73584×10^{-11}	2.09112×10^{-9}	1.30324×10^{-10}	2.09907×10^{-7}
	1	4.31727×10^{-10}	1.43554×10^{-7}	5.20385×10^{-10}	9.30101×10^{-12}
4	0.2	8.86264×10^{-13}	1.00258×10^{-6}	2.61299×10^{-14}	2.02384×10^{-10}
	0.4	2.23943×10^{-12}	2.44714×10^{-9}	5.03161×10^{-13}	1.47209×10^{-9}
	0.6	1.70319×10^{-12}	3.18751×10^{-9}	3.65031×10^{-12}	7.11536×10^{-9}
	0.8	9.11656×10^{-12}	2.83350×10^{-10}	1.76376×10^{-11}	2.84106×10^{-8}
	1	5.84287×10^{-11}	1.94306×10^{-8}	7.04272×10^{-11}	1.25588×10^{-12}

Table 4. Numerical values of approximate solution of Example 3 at $x = 0.9$ and $l = 10$ for different α.

ξ	η	α = 0.75			α = 1		
		GB-HPM	NTDM [49]	q-HATM [50]	GB-HPM	NTDM [49]	q-HATM [50]
1	0.2	0.031802	0.031802	0.031793	0.031446	0.031446	0.031446
	0.4	0.032452	0.032452	0.032452	0.032007	0.032008	0.032007
	0.6	0.033051	0.033051	0.033051	0.032587	0.032587	0.032587
	0.8	0.033627	0.033627	0.033627	0.033187	0.033187	0.033187
	1	0.034191	0.034191	0.034191	0.033810	0.033810	0.033810
2	0.2	0.060430	0.060430	0.060430	0.059780	0.059780	0.059780
	0.4	0.061608	0.061608	0.061608	0.060807	0.060807	0.060806
	0.6	0.062681	0.062681	0.062681	0.061860	0.061860	0.061860
	0.8	0.063701	0.063701	0.063701	0.062942	0.062942	0.062942
	1	0.064692	0.064692	0.064692	0.064055	0.064055	0.064055
3	0.2	0.083072	0.083072	0.083072	0.082224	0.082224	0.082224
	0.4	0.084594	0.084594	0.085442	0.083568	0.083568	0.083568
	0.6	0.085958	0.085958	0.087236	0.084933	0.084933	0.084933
	0.8	0.087236	0.087236	0.088458	0.086321	0.086321	0.086321
	1	0.088458	0.088459	0.097559	0.087732	0.087732	0.087731
4	0.2	0.097559	0.097559	0.099254	0.096607	0.096607	0.096607
	0.4	0.099254	0.099254	0.100751	0.098121	0.098121	0.098121
	0.6	0.100751	0.100751	0.102134	0.099646	0.099646	0.099646
	0.8	0.102134	0.102134	0.103439	0.101181	0.101181	0.101181
	1	0.103439	0.103439	0.102541	0.102725	0.102725	0.102725

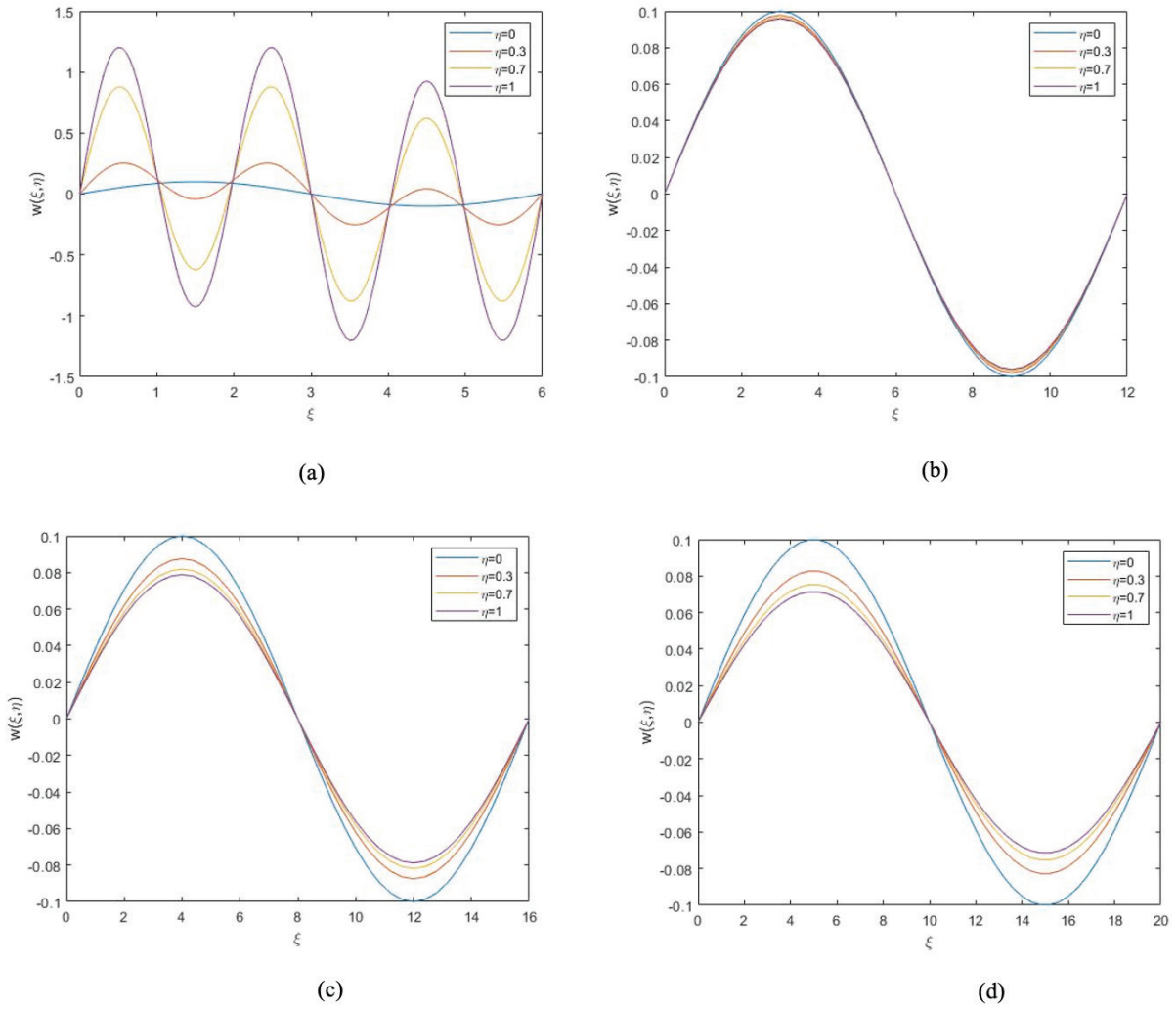

Figure 5. Solution profile of GB-HPM solution for Example 3 when $\alpha = 0.5$ and $x = 0.5$ at (a) $l = 3$ (b) $l = 6$ (c) $l = 8$ (d) $l = 10$.

Table 5. Absolute error in consecutive approximate solutions of Example 3 at $x = 0.9$ and $l = 10$ for $\alpha = 0.75$

ξ	η	$\lvert W_2 - W_1 \rvert$	$\lvert W_3 - W_2 \rvert$	$\lvert W_4 - W_3 \rvert$
1	0.01	2.92569×10^{-7}	2.59836×10^{-9}	3.01272×10^{-11}
	0.1	9.25185×10^{-6}	4.62061×10^{-7}	3.01272×10^{-8}
	0.5	1.03439×10^{-4}	1.72736×10^{-5}	3.76590×10^{-6}
2	0.01	4.30788×10^{-7}	3.09033×10^{-9}	3.49638×10^{-11}
	0.1	1.36227×10^{-5}	5.49547×10^{-7}	3.49638×10^{-8}
	0.5	1.52307×10^{-4}	2.05441×10^{-5}	4.37047×10^{-6}
3	0.01	3.82210×10^{-7}	1.10898×10^{-9}	1.07566×10^{-11}
	0.1	1.20866×10^{-5}	1.97208×10^{-7}	1.07566×10^{-8}
	0.5	1.35132×10^{-4}	7.37238×10^{-6}	1.34457×10^{-6}
4	0.01	2.51909×10^{-7}	1.68264×10^{-9}	2.19749×10^{-11}
	0.1	7.96607×10^{-6}	2.99221×10^{-7}	2.19749×10^{-8}
	0.5	8.90633×10^{-5}	1.11860×10^{-5}	2.74687×10^{-6}

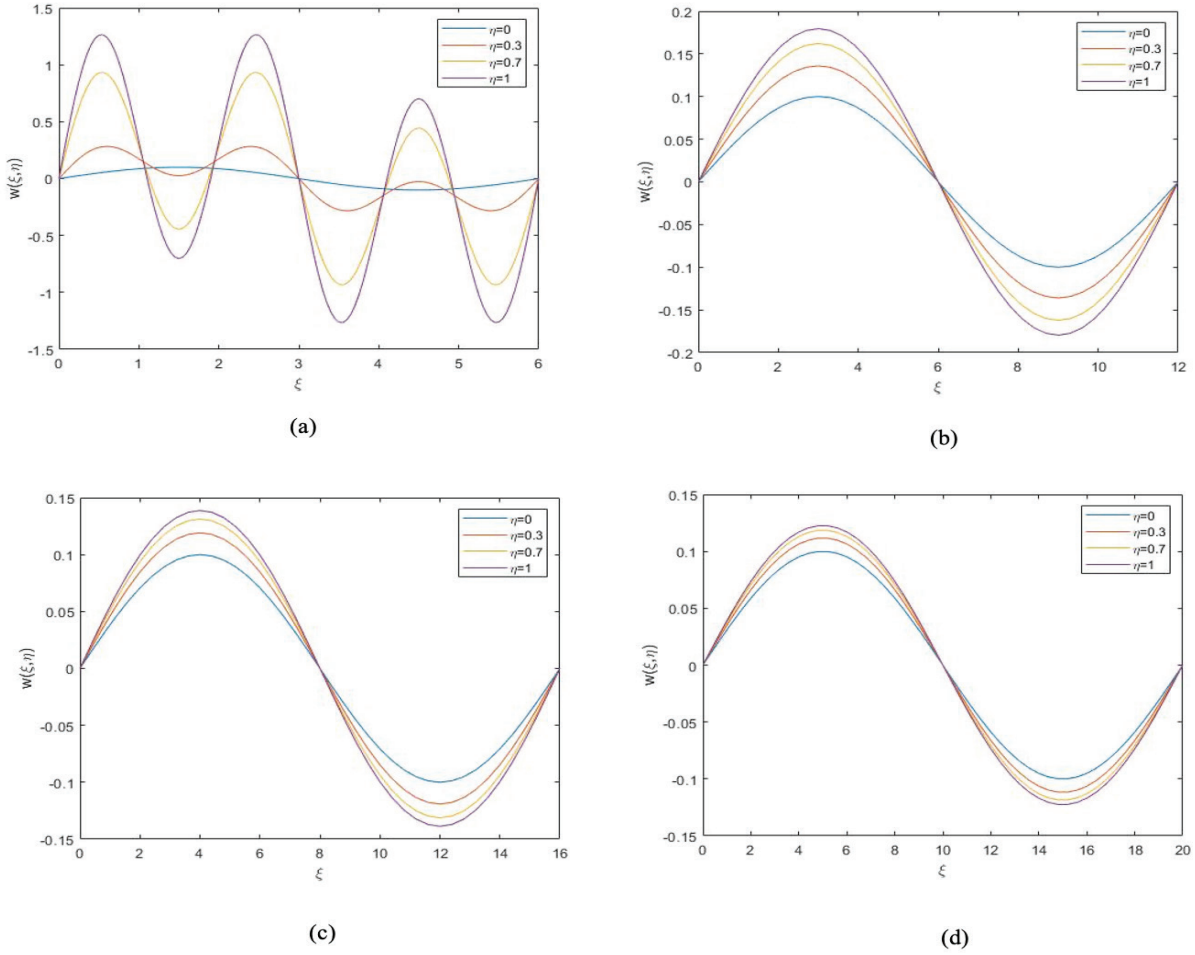

Figure 6. Solution profile of GB-HPM solution for Example 3 when $\alpha = 0.5$ and $x = 1$ at (a) $l = 3$ (b) $l = 6$ (c) $l = 8$ (d) $l = 10$.

Table 6. Numerical values of approximate solution of Example 4 at $x = 0.5$, $y = 0.7$ and $l = 10$ for different α

ξ	η	α = 0.75			α = 1		
		GB-HPM	NTDM [49]	q-HATM [50]	GB-HPM	NTDM [49]	q-HATM [50]
1	0.2	0.041383	0.041383	0.042774	0.036887	0.036887	0.037301
	0.4	0.050226	0.050226	0.054156	0.043729	0.043729	0.045381
	0.6	0.059170	0.059170	0.066390	0.051459	0.051459	0.055176
	0.8	0.068403	0.068403	0.079519	0.060108	0.060108	0.066716
	1	0.077989	0.077989	0.093524	0.069706	0.069706	0.080031
2	0.2	0.082115	0.082115	0.086069	0.071563	0.071563	0.072738
	0.4	0.104496	0.104496	0.115681	0.087199	0.087199	0.091901
	0.6	0.129531	0.129531	0.150079	0.106187	0.106187	0.116767
	0.8	0.157701	0.157701	0.189337	0.129029	0.129029	0.147837
	1	0.189231	0.189231	0.233444	0.156224	0.156224	0.185611
3	0.2	0.115950	0.115950	0.122485	0.099716	0.099716	0.101658
	0.4	0.151505	0.151505	0.169987	0.123489	0.123489	0.131258
	0.6	0.192814	0.192814	0.226768	0.153296	0.153296	0.170778
	0.8	0.240654	0.240654	0.292929	0.190213	0.190213	0.221290
	1	0.295424	0.295424	0.368481	0.235313	0.235313	0.283872
4	0.2	0.138479	0.138479	0.146962	0.118122	0.118122	0.120643
	0.4	0.183832	0.183832	0.207824	0.147741	0.147741	0.157827
	0.6	0.237549	0.237549	0.281626	0.185526	0.185526	0.208219
	0.8	0.300634	0.300634	0.368495	0.233036	0.233036	0.273379
	1	0.373628	0.373628	0.468467	0.291832	0.291832	0.354869

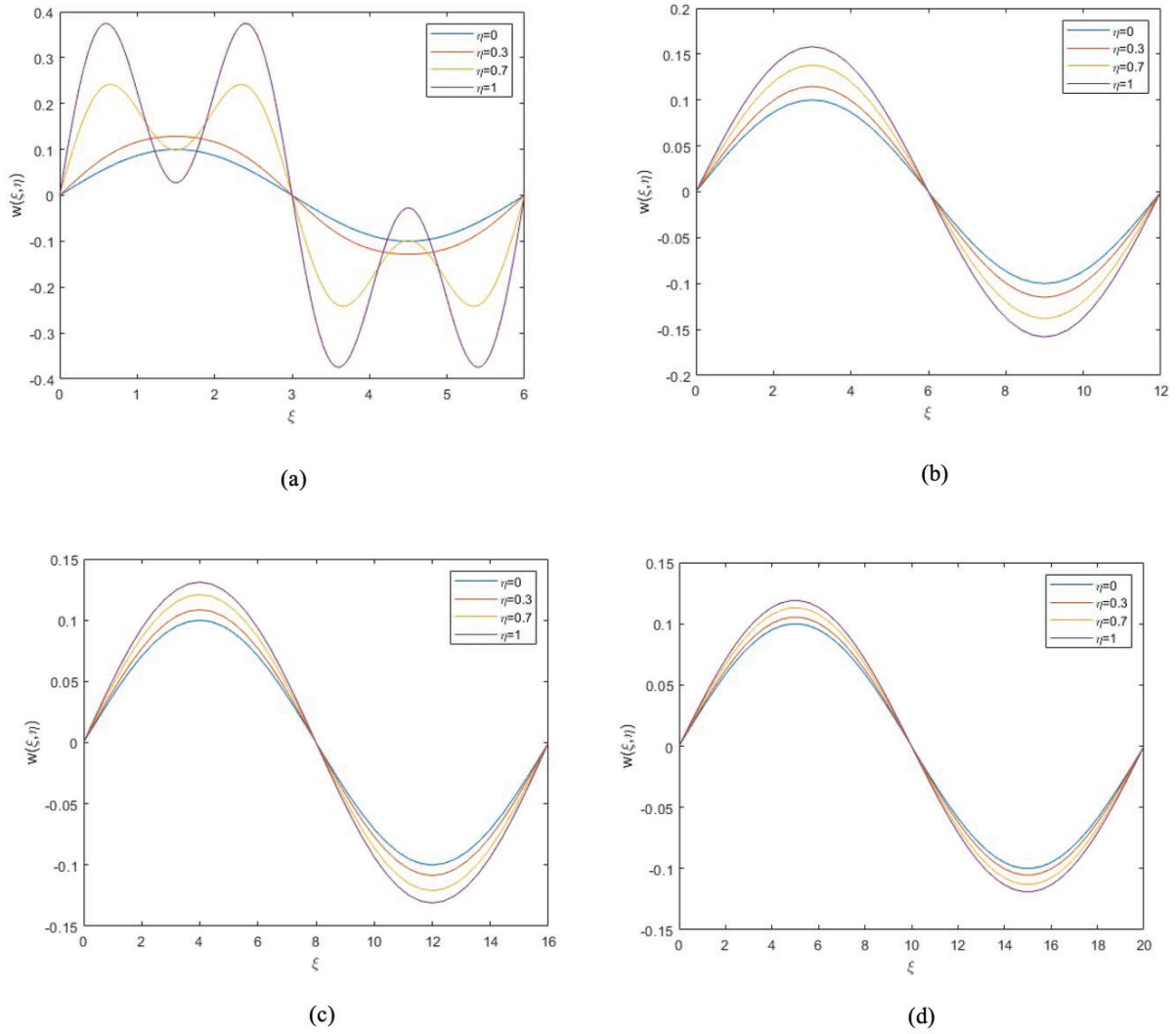

Figure 7. Solution profile of GB-HPM solution for Example 3 when $\alpha = 1$ and $x = 1$ at (a) $l = 3$ (b) $l = 6$ (c) $l = 8$ (d) $l = 10$.

Table 7. Absolute error for approximate solution of Example 5 at $x = 1$ and $\alpha = 1$

ξ	η	GB-HPM	Q-HAM [78]	
0.01	0	2.356974×10^{-12}	2.356975×10^{-12}	-
	1	2.823764×10^{-10}	2.823765×10^{-10}	-
	2	5.749510×10^{-11}	5.749512×10^{-11}	-
	3	3.757251×10^{-11}	3.757261×10^{-11}	-
0.1	0	2.352262×10^{-7}	2.352262×10^{-7}	-
	1	2.722916×10^{-6}	2.722916×10^{-6}	-
	2	5.848640×10^{-7}	5.848640×10^{-7}	-
	3	3.686350×10^{-7}	3.686350×10^{-7}	-
			RPS [76], HPM [79]	**HPM [77]**
0.2	0.1	2.55541×10^{-5}	2.55541×10^{-5}	4.68338×10^{-3}
	0.2	4.15291×10^{-5}	4.15291×10^{-5}	7.28902×10^{-3}
	0.3	5.42246×10^{-5}	5.42246×10^{-5}	9.61620×10^{-3}
	0.4	6.28898×10^{-5}	6.28898×10^{-5}	1.15931×10^{-2}
	0.5	6.72637×10^{-5}	6.72637×10^{-5}	1.31740×10^{-2}

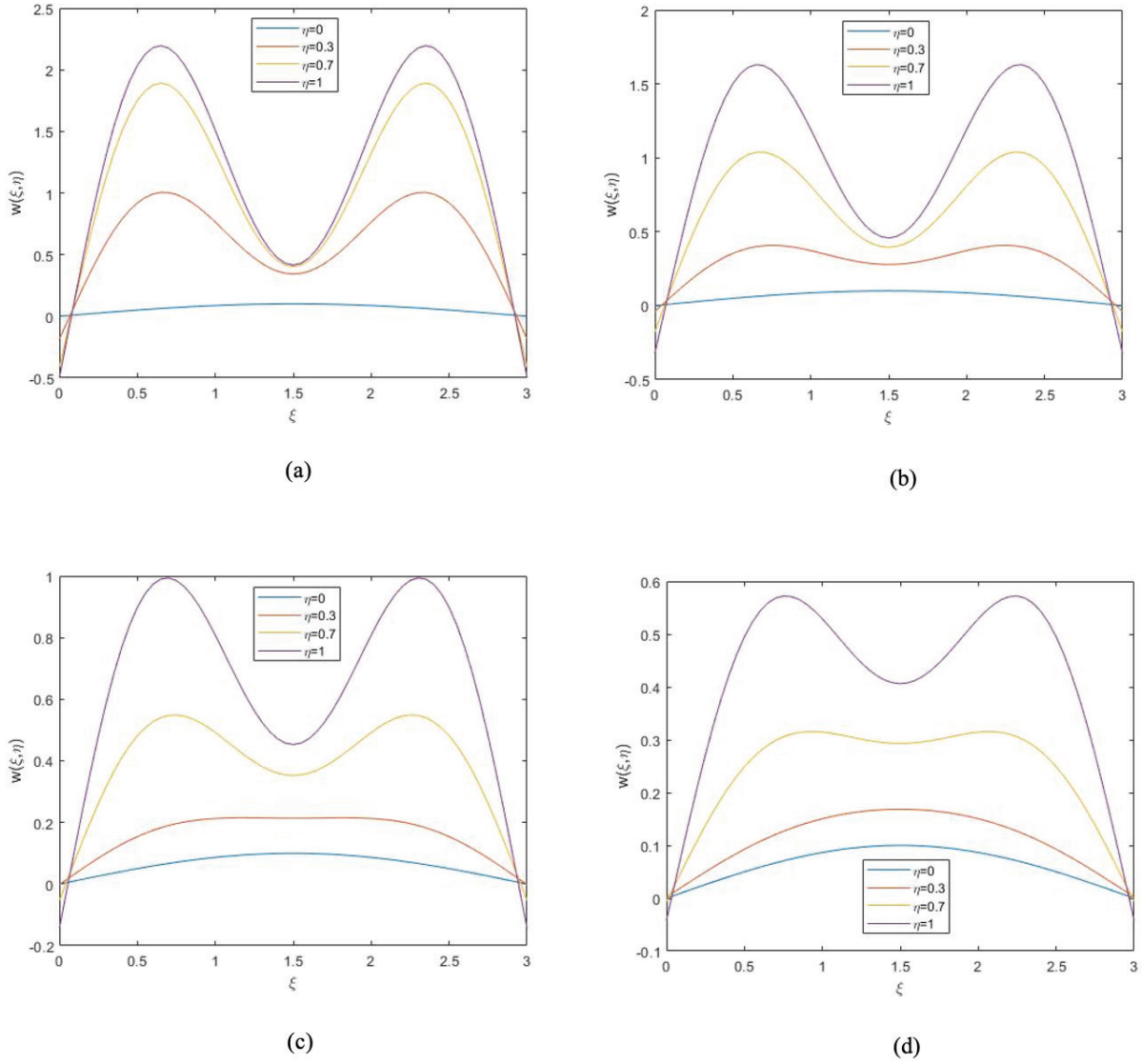

Figure 8. Solution profile of GB-HPM solution for Example 4 when $x = 0$, $y = 0.7$ and $l = 3$ at (a) $\alpha = 0.25$ (b) $\alpha = 0.5$ (c) $\alpha = 0.75$ (d) $\alpha = 1$.

Table 8. Absolute error in consecutive approximate solutions of Example 5 at x =1 and $\alpha = 0.75$

ξ	η	$\lvert W_2 - W_1 \rvert$	$\lvert W_3 - W_2 \rvert$	$\lvert W_4 - W_3 \rvert$
-5	0.01	2.54697×10^{-6}	5.99187×10^{-8}	7.61024×10^{-10}
	0.03	1.32344×10^{-5}	7.09717×10^{-7}	2.05477×10^{-8}
	0.05	2.84759×10^{-5}	2.23998×10^{-6}	9.51280×10^{-8}
-2	0.01	1.40856×10^{-4}	4.04291×10^{-6}	1.16966×10^{-6}
	0.03	7.31911×10^{-4}	4.78869×10^{-5}	3.15809×10^{-5}
	0.05	1.57482×10^{-3}	1.51139×10^{-4}	1.46208×10^{-4}
2	0.01	1.40856×10^{-4}	1.01417×10^{-6}	9.74371×10^{-7}
	0.03	7.31911×10^{-4}	1.20124×10^{-5}	2.63080×10^{-5}
	0.05	1.57482×10^{-3}	3.79133×10^{-5}	1.21796×10^{-4}
5	0.01	2.54697×10^{-6}	5.84709×10^{-8}	5.89081×10^{-10}
	0.03	1.32344×10^{-5}	6.92568×10^{-7}	1.59052×10^{-8}
	0.05	2.84759×10^{-5}	2.18586×10^{-6}	7.36351×10^{-8}

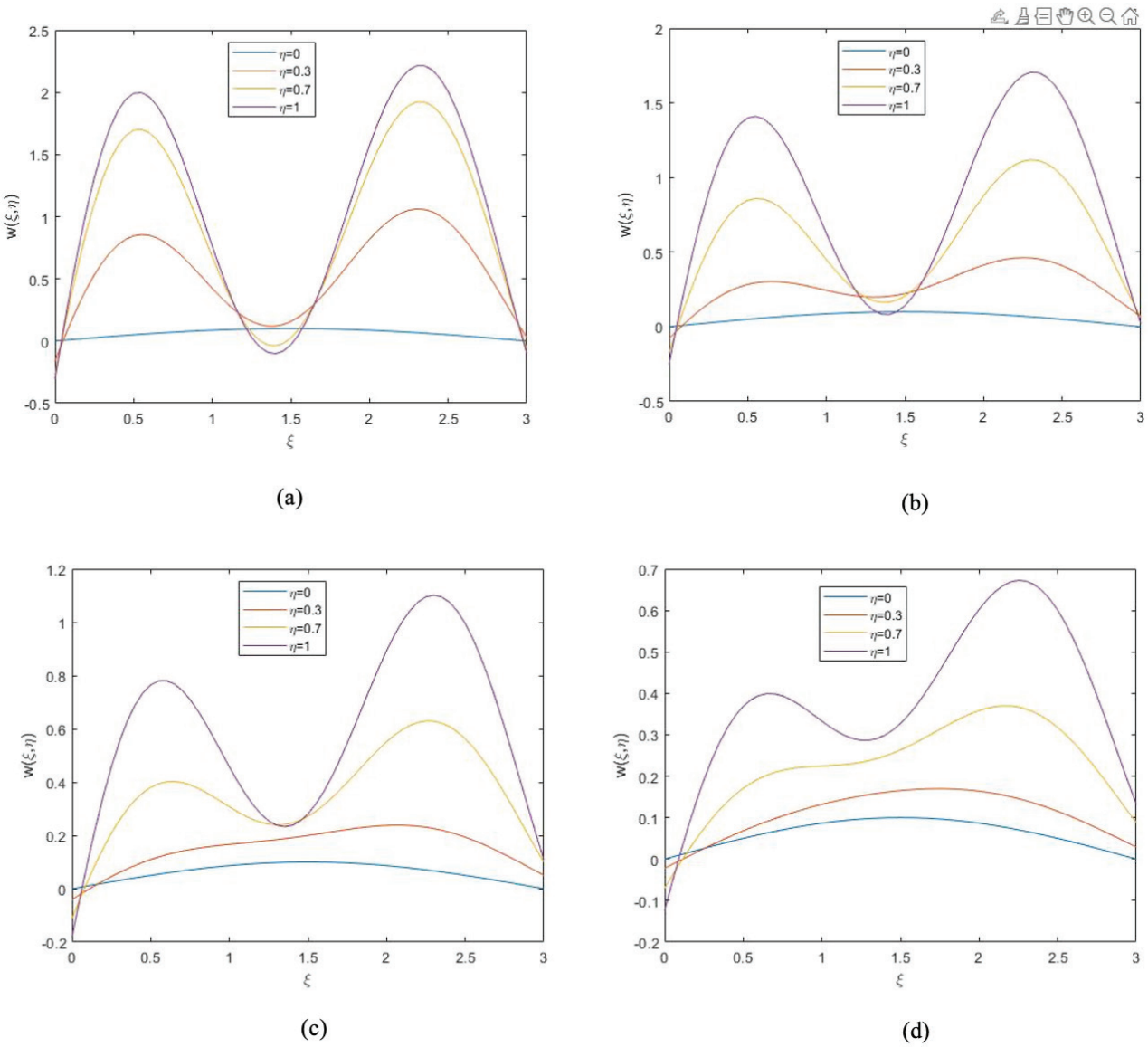

Figure 9. Solution profile of GB-HPM solution for Example 4 when $x = 0.5$, $y = 0.7$ and $l = 3$ at (a) $\alpha = 0.25$ (b) $\alpha = 0.5$ (c) $\alpha = 0.75$ (d) $\alpha = 1$.

and so on. The graphical illustrations for obtained GB-HPM solution to analyze the effect of dispersion and bifurcation parameters (i.e., x and y, respectively) on probability density function $w(\xi,\eta)$ have been presented in Figure 8, Figure 9, Figure 10 and Figure 11. From comparative visualization of presented figures for Example 4, it can be stated that $w(\xi,\eta)$ has a significant effect of included physical parameters for $l = 3$. However, for $l = 10$ solution profile does not depict much difference with respect to the variation in x and y. The presented figures also exhibit the evolution of solution profile with an increase in time for different values of fractional order α. Numerical values tabulated in Table 6 again demonstrate the agreement of GB-HPM solution with NTDM [49] and q-HATM [50] solutions.

Example 5. Consider FCH with the initial data $w(\xi,0) = tanh\left(\frac{\sqrt{2}}{2}x\right)$ and for $x = 1$ on setting $\alpha = 1$ the corresponding exact solution is given by:

$$w(\xi,\eta) = tanh\left(\frac{\sqrt{2}}{2}(\xi+\eta)\right). \tag{37}$$

Following the criteria of proposed framework with choice of

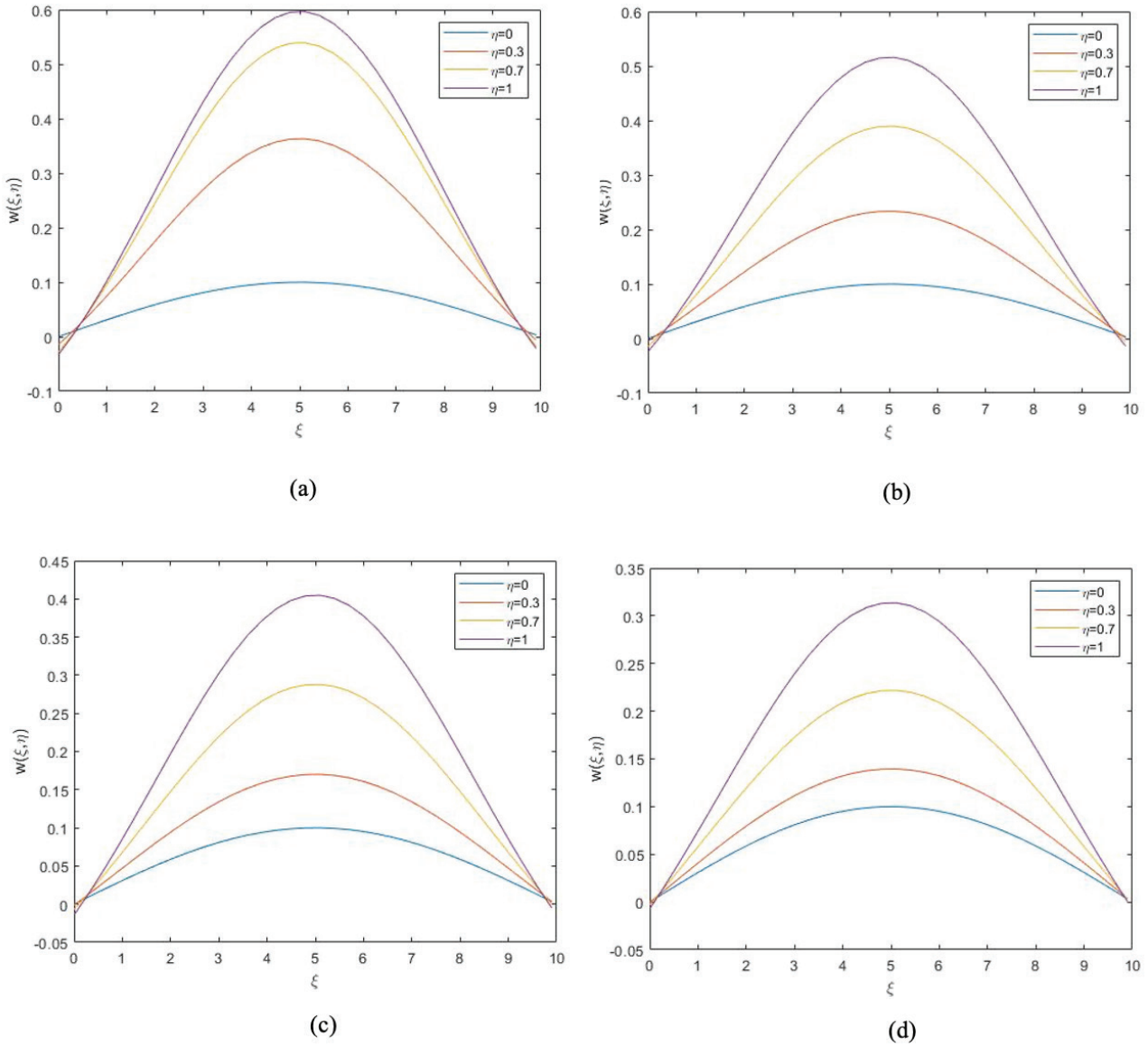

Figure 10. Solution profile of GB-HPM solution for Example 4 when $x = 0$, $y = 0.7$ and $l = 10$ at (a) $\alpha = 0.25$ (b) $\alpha = 0.5$ (c) $\alpha = 0.75$ (d) $\alpha = 1$.

$$\mathcal{P}[w(\xi,\eta)] = xw_{\xi} - w_{\xi\xi} - w_{\xi\xi\xi\xi},$$
$$\mathcal{Q}[w(\xi,\eta)] = 6ww_{\xi}^2 + 3w^2w_{\xi\xi} \; and \; \mathcal{N}(\xi,\eta) = 0,$$

the components of series solution can be obtained as:

$$w_0(\xi,\eta) = tanh\left((\sqrt{2}\xi)/2\right),$$

$$w_1(\xi,\eta) = (\sqrt{2}\eta^{\alpha})/\left(\Gamma(\alpha+1)(cosh(\sqrt{2}\xi)+1)\right),$$

$$w_2(\xi,\eta) = \left(\eta^{2\alpha}sinh\left((\sqrt{2}\xi)/2\right)\right)/\left(\Gamma(2\alpha+1)cosh\left((\sqrt{2}\xi)/2\right)^3\right)\ldots.$$

Continuing the same procedure, the remaining components of the series solution $W_n(\xi,\eta)$ $(n \geq 3)$ can be obtained.

Figure 12 depicts the geometrical configuration of the obtained semi-analytic solution at variant fractional orders. This Figure 12 suggests that the implementation of the proposed method is significantly efficient in finding a smooth wave solution to the specified problem. Surface plots of obtained solution describe the configuration of a kink wave. This wave represents a localized solution that rises or descends from one asymptotic state to another. In phase separation process, the solution profile of Cahn-Hilliard quantifies the transition of concentration of one of the two metallic components of the alloy. The present solution displays the stationary transition of phase in spinodal interval of $|w| < 1$, which directs to the unstable stationary state [75].

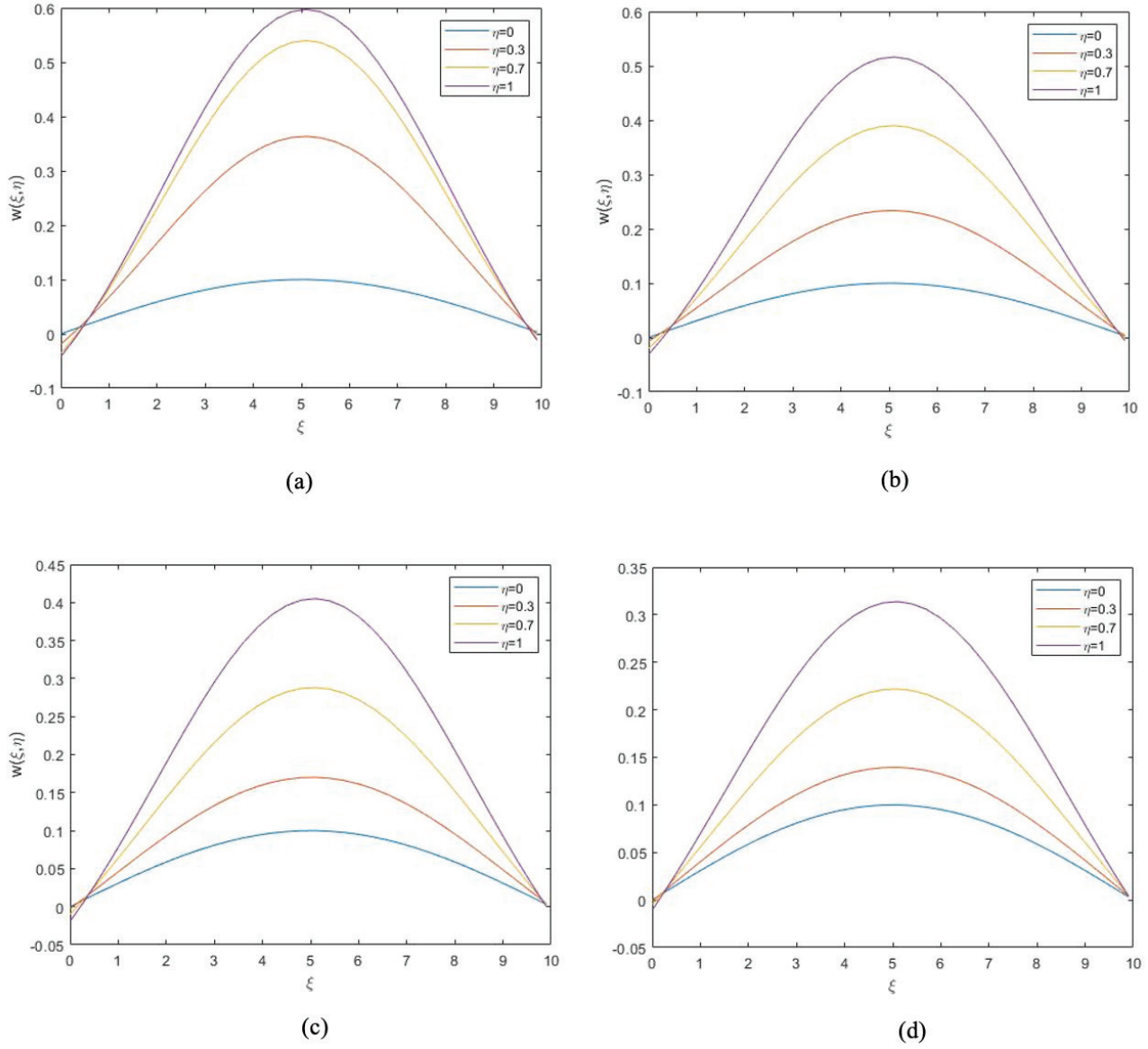

Figure 11. Solution profile of GB-HPM solution for Example 4 when $x = 0.5$, $y = 0.7$ and $l = 10$ at (a) $\alpha = 0.25$ (b) $\alpha = 0.5$ (c) $\alpha = 0.75$ (d) $\alpha = 1$.

In Table 7, a quantitative response of the achieved results in comparison of RPS [76], HPM [77] and q-HAM [78] is presented. For $x = 1$ obtained solution has acquired alike accuracy to RPS and q-HAM. In [76], RPS is found superior to HPM for solving fractional C-H equation. For the case $\alpha = 1$, the obtained solution converges to the solution obtained for the classical C-H equation, utilizing HPM and ADM [79]. Therefore, the GB transform can be considered a convergence booster of classical HPM for fractional equations. In addition, Table 8 reveals the convergence phenomenon with rapidly diminishing errors of consecutive approximations with increasing n for $\alpha = 0.75$. The consistency in terms of accuracy of the approximate solution in both cases of fractional and integer order equations confirms the efficiency of the proposed method.

CONCLUSION

In this article, the time-fractional generalized Kuramoto-Sivashinsky equation, Swift-Hohenberg equation, Cahn-Hilliard equation, and their special cases have been studied using the semi-analytic generalized bivariate homotopy perturbation method. Dynamics of several waveforms have been analyzed for different values of fractional order and physical parameters. Existence and uniqueness are presented for continuous solutions of fractional variants

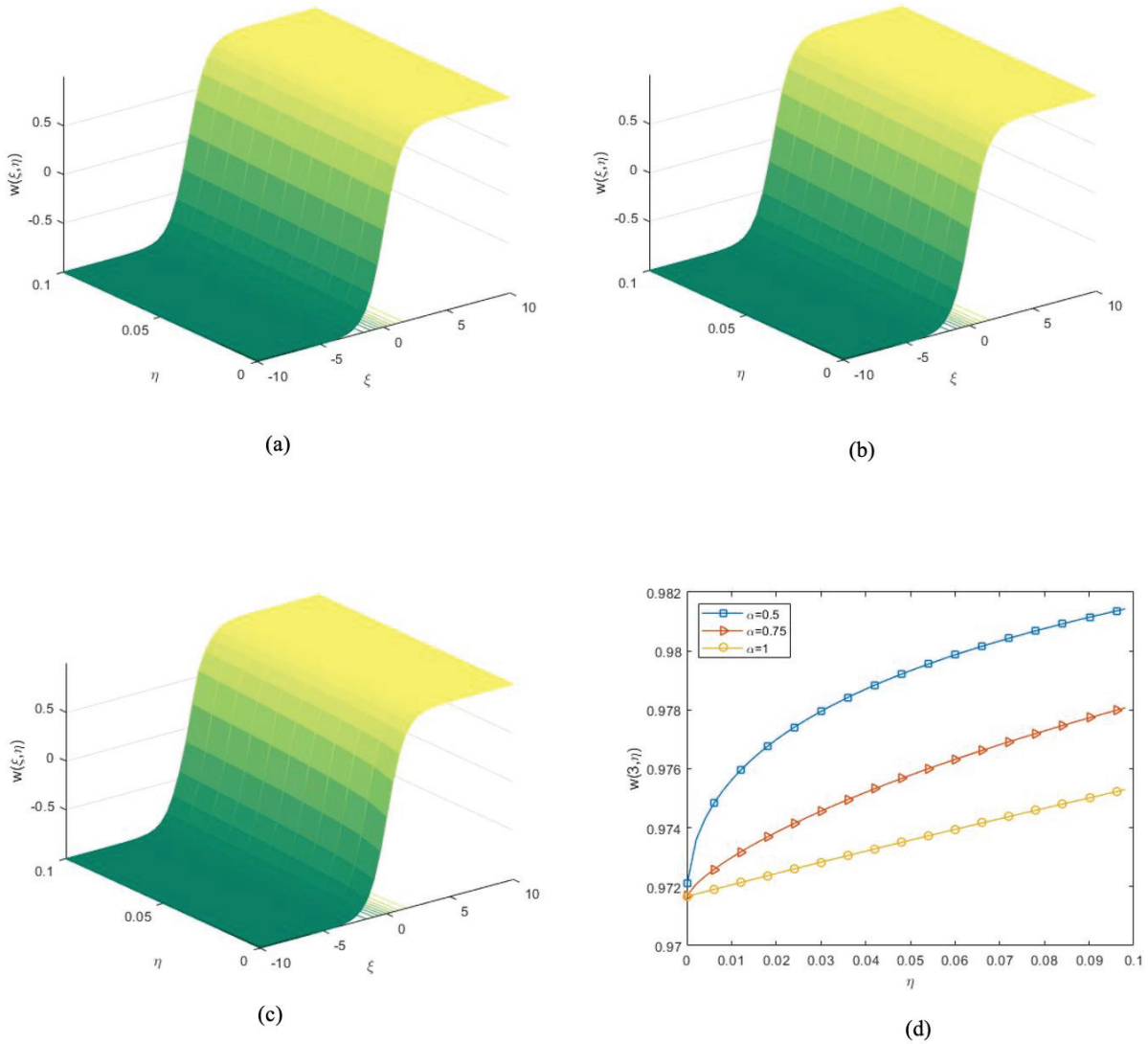

Figure 12. Solution profile of GB-HPM solution for Example 5 when x = 1 at (a) α = 0.5 (b) α = 0.75 (c) α = 1 (d) ξ = 3.

of Kuramoto-Sivashinsky, Swift-Hohenberg and Cahn-Hilliard equations. The suggested method is free from the assumption of requiring major or minor physical parameters in the problem. The graphical illustrations and tabulated absolute error of given results in contrast to existing analytic results establish the worthiness of the proposed scheme. While addressing non-linear problems by generalized bivariate homotopy perturbation method, the assessment of He's polynomials is much easier than the Adomain's polynomials. Generalized bivariate homotopy perturbation method is found highly competent in targeting fractional order challenges. Another advantage is that this method does not require any discretization of variables or linearization of non-linear terms, which preserves actual non-linear effects, large computer memory and extensive time. Beyond this, generalized bivariate homotopy perturbation method does not require exact solution to prove its credibility. For aspects of further advancements, the application of the proposed scheme to stochastic, hyperbolic and higher-dimensional systems can provide good supplements to the existing literature.

ACKNOWLEDGEMENT

Shelly Arora is thankful to SERB-POWER for grant support to complete this research via grant number SPG/2022/001269.

AUTHORSHIP CONTRIBUTIONS

Authors equally contributed to this work.

DATA AVAILABILITY STATEMENT

The authors confirm that the data that supports the findings of this study are available within the article.

CONFLICT OF INTEREST

The author declared no potential conflicts of interest with respect to the research, authorship, and/or publication of this article.

ETHICS

There are no ethical issues with the publication of this manuscript

REFERENCES

[1] Çulha Ünal S. Approximate solutions of the fractional Harry Dym equation. Sigma J Eng Nat Sci 2024;42:1604–1611. [CrossRef]

[2] İskenderoğlu G, Kaya D. Lie symmetry analysis of Caputo time-fractional K(m,n) model equations with variable coefficients. Sigma J Eng Nat Sci 2024;42:885–899. [CrossRef]

[3] Merdan M, Öktem S. On solutions of time fractional order random HIV/AIDS modelling. Sigma J Eng Nat Sci 2024;42:1899–1906. [CrossRef]

[4] Günerhan H, Kaabar MK, Çelik E. Novel analytical and approximate-analytical methods for solving the nonlinear fractional smoking mathematical model. Sigma J Eng Nat Sci 2023;41:331–343.

[5] Yépez-Martínez H, Gómez-Aguilar F, Sosa IO, Reyes JM, Torres-Jiménez J. The Feng's first integral method applied to the nonlinear mKdV space-time fractional partial differential equation. Rev Mex Fis 2016;62:310–316. [CrossRef]

[6] Baleanu D, Machado JA, Luo AC. Fractional dynamics and control. New York: Springer; 2011. [CrossRef]

[7] Magin RL. Fractional calculus in bioengineering. Crit Rev Biomed Eng 2004;32:1–104. [CrossRef]

[8] Ellahi R, Alamri SZ, Basit A, Majeed A. Effects of MHD and slip on heat transfer boundary layer flow over a moving plate based on specific entropy generation. J Taibah Univ Sci 2018;12:476–482. [CrossRef]

[9] Li C, Qian D, Chen Y. On Riemann-Liouville and Caputo derivatives. Discrete Dyn Nat Soc 2011;2011:562494. [CrossRef]

[10] Tenreiro-Machado JA, Silva MF, Barbosa RS, Jesus IS, Reis CM, Marcos MG, Galhano AF. Some applications of fractional calculus in engineering. Math Prob Eng 2010;2010:639801. [CrossRef]

[11] Lotfi A, Dehghan M, Yousefi SA. A numerical technique for solving fractional optimal control problems. Comput Math Appl 2011;62:1055–1067. [CrossRef]

[12] Engheia N. On the role of fractional calculus in electromagnetic theory. IEEE Antennas Propag Mag 1997;39:35–46. [CrossRef]

[13] Cruz-Duarte JM, Rosales-Garcia J, Correa-Cely CR, Garcia-Perez A, Avina-Cervantes JG. A closed form expression for the Gaussian–based Caputo–Fabrizio fractional derivative for signal processing applications. Commun Nonlinear Sci Numer Simul 2018;61:138–148. [CrossRef]

[14] Sweilam NH, Abou Hasan MM, Baleanu D. New studies for general fractional financial models of awareness and trial advertising decisions. Chaos Solitons Fractals 2017;104:772–784. [CrossRef]

[15] Kilbas AA, Srivastava HM, Trujillo JJ. Theory and applications of fractional differential equations. Amsterdam: Elsevier; 2006.

[16] Diethelm K, Garrappa R, Giusti A, Stynes M. Why fractional derivatives with non-singular kernels should not be used. Fract Calc Appl Anal 2020;23:610–634. [CrossRef]

[17] Aydın M. An explicit solution of linear conformable systems with variable coefficients. Sigma J Eng Nat Sci 2024;42:1806–1812. [CrossRef]

[18] Ansar R, Abbas M, Mohammed PO, Al-Sarairah E, Gepreel KA, Soliman MS. Dynamical study of coupled Riemann wave equation involving conformable, beta, and M-truncated derivatives via two efficient analytical methods. Symmetry 2023;15:1293. [CrossRef]

[19] Lakestani M, Dehghan M. Numerical solutions of the generalized Kuramoto–Sivashinsky equation using B-spline functions. Appl Math Model 2012;36:605–617. [CrossRef]

[20] Zayed EM, Nofal TA, Gepreel KA. The travelling wave solutions for non-linear initial-value problems using the homotopy perturbation method. Int J Control 2009;88:617–634. [CrossRef]

[21] Song L, Zhang H. Application of homotopy analysis method to fractional KdV–Burgers–Kuramoto equation. Phys Lett A 2007;367:88–94. [CrossRef]

[22] Yin W, Xu F, Zhang W, Gao Y. Asymptotic expansion of the solutions to time-space fractional Kuramoto-Sivashinsky equations. Adv Math Phys 2016;2016:4632163. [CrossRef]

[23] Shah R, Khan H, Baleanu D, Kumam P, Arif M. A semi-analytical method to solve family of Kuramoto–Sivashinsky equations. J Taibah Univ Sci 2020;14:402–411. [CrossRef]

[24] Veeresha P, Prakasha D. Solution for fractional Kuramoto–Sivashinsky equation using novel computational technique. Int J Appl Comput Math 2021;7:33. [CrossRef]

[25] Ebadi G, Biswas A. Application of G'/G–expansion method to Kuramoto–Sivashinsky equation. Acta Math Appl Sin Engl Ser 2016;32:623–630. [CrossRef]

[26] Nazari-Golshan A. Fractional generalized Kuramoto-Sivashinsky equation: Formulation and solution. Eur Phys J Plus 2019;134:565. [CrossRef]

[27] Noor MA, Mohyud-Din ST, Waheed A. Exp-function method for solving Kuramoto–Sivashinsky and Boussinesq equations. J Appl Math Comput 2009;29:1–13. [CrossRef]

[28] Kilicman A, Silambarasan R. Modified Kudryashov method to solve generalized Kuramoto-Sivashinsky equation. Symmetry 2018;10:527. [CrossRef]
[29] Wazwaz AM. New solitary wave solutions to the Kuramoto-Sivashinsky and the Kawahara equations. Appl Math Comput 2006;82:1642–1650. [CrossRef]
[30] Sahoo S, Ray SS. New approach to find exact solutions of time fractional Kuramoto–Sivashinsky equation. Physica A 2015;434:240–245. [CrossRef]
[31] Conte R, Musette M. Painleve analysis and Backlund transformation in the Kuramoto-Sivashinsky equation. J Phys A Math Gen 1989;22:169. [CrossRef]
[32] Hyman JM, Nicolaenko B. The Kuramoto-Sivashinsky equation: A bridge between PDEs and dynamical systems. Physica D Nonlinear Phenomena 1986;18:113–126. [CrossRef]
[33] Hooper A, Grimshaw R. Travelling wave solutions of the Kuramoto-Sivashinsky equation. Wave Motion 1988;10:405–420. [CrossRef]
[34] Frisch U, She ZS, Thual O. Viscoelastic behaviour of cellular solutions to the Kuramoto-Sivashinsky model. J Fluid Mech 1986;168:221–240. [CrossRef]
[35] Abdel-Gawad HI, Abdusalam HA. Approximate solutions of the Kuramoto–Sivashinsky equation for periodic boundary value problems and chaos. Chaos Solitons Fractals 2001;12:2039–2050. [CrossRef]
[36] Swift J, Hohenberg PC. Hydrodynamic fluctuations at the convective instability. Phys Rev A 1977;15:319–328. [CrossRef]
[37] Malygin G. Mechanism of the formation of shear microbands under plastic deformation of nanocrystalline materials. Phys Solid State 2009;51:1814–1820. [CrossRef]
[38] Bodenschatz E, Pesch W, Ahlers G. Recent developments in Rayleigh-Bénard convection. Annu Rev Fluid Mech 2000;32:709–778. [CrossRef]
[39] Lega J, Moloney JV, Newell AC. Swift-Hohenberg equation for lasers. Phys Rev Lett 1994;73:2978. [CrossRef]
[40] Blair D, Aranson IS, Crabtree GW, Vinokur V, Tsimring LS, Josserand C. Patterns in thin vibrated granular layers: Interfaces, hexagons, and superoscillons. Phys Rev E 2000;61:5600. [CrossRef]
[41] Peletier LA, Rottschäfer V. Large time behaviour of solutions of the Swift–Hohenberg equation. C R Math 2003;336:225–230. [CrossRef]
[42] Fife PC. Pattern formation in gradient systems. In: Handbook of Dynamical Systems 2. Amsterdam: Elsevier Science; 2002.
[43] Hoyle RB. Pattern formation: An introduction to methods. Cambridge University Press; 2006. [CrossRef]
[44] Mandel P. Theoretical problems in cavity nonlinear optics. Cambridge University Press; 2005.
[45] Ryabov PN, Kudryashov NA. Non-linear waves described by the generalized Swift-Hohenberg equation. J Phys Conf Ser 2017;788:012032. [CrossRef]
[46] Braaksma B, Iooss G, Stolovitch L. Proof of quasipatterns for the Swift–Hohenberg equation. Commun Math Phys 2017;353:37–67. [CrossRef]
[47] Burke J, Houghton SM, Knobloch E. Swift-Hohenberg equation with broken reflection symmetry. Phys Rev E Stat Nonlinear Soft Matter Phys 2009;80:036202. [CrossRef]
[48] Kudryashov NA, Sinelshchikov DI. Exact solutions of the Swift–Hohenberg equation with dispersion. Commun Nonlinear Sci Numer Simul 2012;17:26–34. [CrossRef]
[49] Pavani K, Raghavendar K. Approximate solutions of time-fractional Swift–Hohenberg equation via natural transform decomposition method. Int J Appl Comput Math 2023;9:29. [CrossRef]
[50] Veeresha P, Prakasha DG, Baleanu D. Analysis of fractional Swift-Hohenberg equation using a novel computational technique. Math Methods Appl Sci 2020;43:1970–1987. [CrossRef]
[51] Almutlak SA, Shah R, Weera W, El-Tantawy SA, El-Sherif LS. Fractional view analysis of Swift-Hohenberg equations by an analytical method and some physical applications. Fractals 2022;6:524. [CrossRef]
[52] Li W, Pang Y. An iterative method for time-fractional Swift-Hohenberg equation. Adv Math Phys 2018;2018:2405432. [CrossRef]
[53] Grasselli M, Schimperna G, Zelik S. On the 2D Cahn–Hilliard equation with inertial term. Commun Partial Differ Equ 2009;34:137–170. [CrossRef]
[54] Lee D, Huh JY, Jeong D, Shin J, Yun A, Kim J. Physical, mathematical, and numerical derivations of the Cahn–Hilliard equation. Comput Mater Sci 2014;81:216–225. [CrossRef]
[55] Chen W, Wang C, Wang X, Wise SM. Positivity-preserving, energy stable numerical schemes for the Cahn-Hilliard equation with logarithmic potential. J Comput Phys X 2019;3:100031. [CrossRef]
[56] Zhang X, Li H, Liu C. Optimal control problem for the Cahn–Hilliard/Allen–Cahn equation with state constraint. Appl Math Optim 2020;82:721–754. [CrossRef]
[57] Storvik E, Both JW, Nordbotten JM, Radu FA. A Cahn–Hilliard–Biot system and its generalized gradient flow structure. Appl Math Lett 2022;126:107799. [CrossRef]
[58] Manzanero J, Redondo C, Rubio G, Ferrer E, Rivero–Jiménez Á. A discontinuous Galerkin approximation for a wall–bounded consistent three–component Cahn–Hilliard flow model. Comput Fluids 2022;225:104971. [CrossRef]
[59] Khan MA, Akbar MA, Binti-Abd-Hamid NN. Traveling wave solutions for space-time fractional Cahn-Hilliard equation and space-time fractional symmetric regularized long-wave equation. Alex Eng J 2021;60:1317–1324. [CrossRef]

[60] Zhou S, Xie YM. Numerical simulation of three-dimensional multicomponent Cahn–Hilliard systems. Int J Mech Sci 2021;198:106349. [CrossRef]
[61] Akgül A, Öztürk G. Application of the Sumudu transform to some equations with fractional derivatives. Sigma J Eng Nat Sci 2023;41:1132–1143. [CrossRef]
[62] Aboodh KS. The new integral transform 'Aboodh transform'. Glob J Pure Appl Math 2013;9:35–43.
[63] Saadeh R, Qazza A, Burqan A. A new integral transform: ARA transform and its properties and applications. Symmetry 2020;12:925. [CrossRef]
[64] Saadeh RZ, Ghazal BF. A new approach on transforms: Formable integral transform and its applications. Axioms 2021;10:332. [CrossRef]
[65] Elzaki TM. The new integral transform Elzaki transform. Glob J Pure Appl Math 2011;7:57–64.
[66] Maitama S, Zhao W. Beyond Sumudu transform and natural transform: J-transform properties and applications. J Appl Anal Comput 2020;10:1223–1241. [CrossRef]
[67] Khan ZH, Khan WA. N-transform properties and applications. Nust J Eng Sci 2008;1:127–133.
[68] Maitama S, Zhao W. New integral transform: Shehu transform a generalization of Sumudu and Laplace transform for solving differential equations. Int J Anal Appl 2019;17:167–190.
[69] Yang XJ. A new integral transform with an application in heat-transfer problem. Therm Sci 2016;20:677–681. [CrossRef]
[70] Arora S, Pasrija A. A novel integral transform operator and its applications. Iran J Numer Anal Optim 2023;13:553–575.
[71] Arora S, Dhaliwal SS, Ma WX, Pasrija A. Analysis of fractional order Schrödinger equation with singular and non-singular kernel derivatives via novel hybrid scheme. J Appl Anal Comput 2025;15:1039–1067. [CrossRef]
[72] Taneco-Hernández MA, Morales-Delgado VF, Gómez-Aguilar JF. Fractional Kuramoto–Sivashinsky equation with power law and stretched Mittag-Leffler kernel. Physica A Stat Mech Appl 2019;527:121085. [CrossRef]
[73] Khan Y, Wu Q. Homotopy perturbation transform method for nonlinear equations using He's polynomials. Comput Math Appl 2011;61:1963–1967. [CrossRef]
[74] Ghorbani A. Beyond Adomian polynomials: He polynomials. Chaos Solitons Fractals 2009;39:1486–1492. [CrossRef]
[75] Taneco-Hernández MA, Morales-Delgado VF, Gómez-Aguilar JF. The Willmore functional and instabilities in the Cahn-Hilliard equation. Commun Math Sci 2008;6:309–329. [CrossRef]
[76] Arafa A, Elmahdy G. Application of residual power series method to fractional coupled physical equations arising in fluids flow. Int J Differ Equ 2018;2018:7692849. [CrossRef]
[77] Bouhassoun A, Hamdi–Cherif M. Homotopy perturbation method for solving the fractional Cahn-Hilliard equation. J Interdiscip Math 2015;18:513–524. [CrossRef]
[78] Akinyemi L, Iyiola OS, Akpan U. Iterative methods for solving fourth and sixth-order time-fractional Cahn-Hillard equation. Math Methods Appl Sci 2020;43:4050–4074. [CrossRef]
[79] Ugurlu Y, Kaya D. Solutions of the Cahn–Hilliard equation. Comput Math Appl 2008;56:3038–3045. [CrossRef